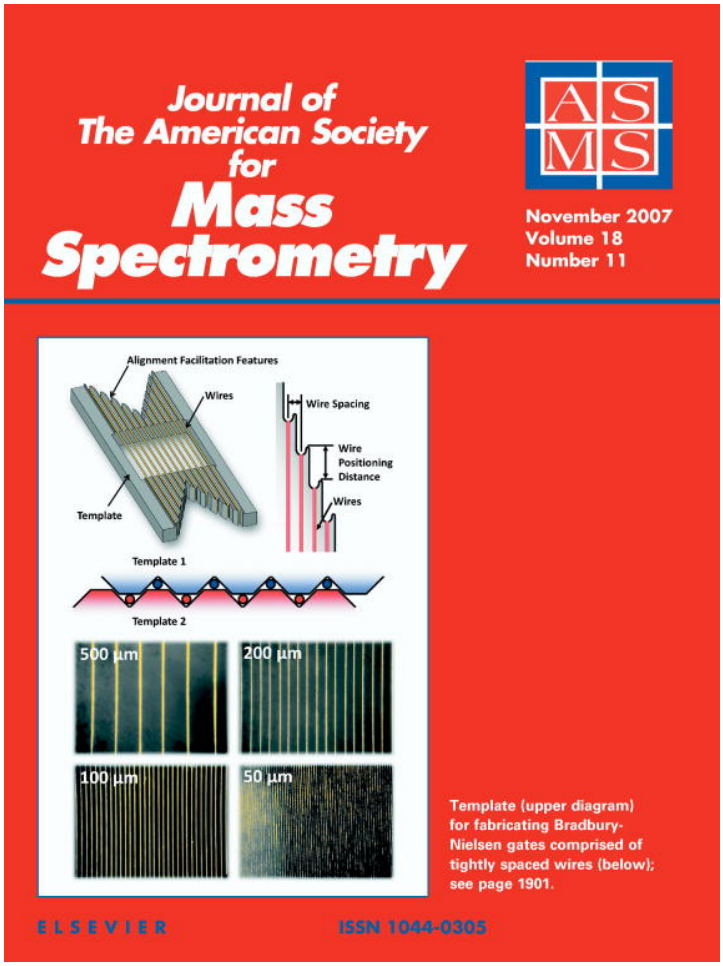

Ammonia Elimination from Protonated Nucleobases and Related Synthetic Substrates

Ming Qian, Shuo Yang, Hong Wu, Papiya Majumdar, Nathan Leigh, and Rainer Glaser

Department of Chemistry, University of Missouri-Columbia, Columbia, Missouri, USA

The results are reported of mass-spectrometric studies of the nucleobases adenine **1h** (**1**, R = H), guanine **2h**, and cytosine **3h**. The protonated nucleobases are generated by electrospray ionization of adenosine **1r** (**1**, R = ribose), guanosine **2r**, and deoxycytidine **3d** (**3**, R = deoxyribose) and their fragmentations were studied with tandem mass spectrometry. In contrast to previous EI-MS studies of the nucleobases, NH_3 elimination does present a major path for the fragmentations of the ions $[\mathbf{1h} + H]^+$, $[\mathbf{2h} + H]^+$, and $[\mathbf{3h} + H]^+$. The ion $[\mathbf{2h} + H - NH_3]^+$ also was generated from the acyclic precursor 5-cyanoamino-4-oxomethylene-dihydroimidazole **13h** and from the thioether derivative **14h** of **2h** (NH_2 replaced by MeS). The analyses of the modes of initial fragmentation is supported by density functional theoretical studies. Conjugate acids **15–55** were studied to determine site preferences for the protonations of **1h**, **2h**, **3h**, **13h**, and **14h**. The proton affinity of the amino group hardly ever is the substrate's best protonation site, and possible mechanisms for NH_3 elimination are discussed in which the amino group serves as the dissociative protonation site. The results provide semi-direct experimental evidence for the existence of the pyrimidine ring-opened cations that we had proposed on the basis of theoretical studies as intermediates in nitrosative nucleobase deamination. (J Am Soc Mass Spectrom 2007, 18, 2040–2057) © 2007 American Society for Mass Spectrometry

Nitric oxide (NO) and nitrous acid (HNO_2) cause DNA base deamination and interstrand cross-link formation [1, 2]. This chemistry has been studied extensively because of the dietary and environmental exposure of humans to these substances [3–5]. Toxicological studies of deamination became more significant when it was recognized that endogenous nitric oxide [6, 7] causes nitrosation [8, 9], and that this process is accelerated by chronic inflammatory diseases [10, 11]. It has been known for a long time that deamination of adenine **1**, guanine **2**, and cytosine **3** (Scheme 1) results in the formation of hypoxanthine, xanthine, and uracil, respectively, and these products are thought to result from DNA base diazonium ions **4–6**, respectively, by direct nucleophilic dediazoniation. The discovery of oxanine formation [12–14] in the nitrosative deamination of guanine challenged the generality and completeness of this mechanism. Theoretical studies revealed that unimolecular dediazoniation of guaninediazonium ion **5** is accompanied or immediately followed by pyrimidine ring-opening [15, 16] and that cytosine-catalysis promotes the process [17, 18]. The resulting 5-cyanoimino-4-oxomethylene-4,5-dihydroimidazole is a highly reactive intermediate and undergoes acid-catalyzed 1,4-addition via cyano-*N* or imino-*N* protonated 5-cyanoimino-4-oxomethylene-4,5-dihydroimidazoles, **9** and **10**, respectively [19]. Labeling studies support this reaction mechanism for oxanine formation [20]. Moreover, we synthesized 5-cyanoamino-4-imidazolecarboxamide and studied its cyclization chemistry [21] and its proficiency for cross-link formation [22]. The unimolecular dediazoniation of the diazonium ions of adenine and cytosine can proceed without ring-opening but the cations **7** and **11** formed in this way are predicted to undergo facile ring-opening [23, 24] to ions **8** and **12**, respectively (Scheme 1).

We reported the results of ab initio studies (MP2/6-31G*) on the electronic structures of ions **9** and **10** and of their common conjugate base and solvent effects were considered by way of a continuum model [19]. The characteristic features of the ions persist in solution, but solvation does have a marked consequence on the site preference and the propensity for protonation. While cyano-*N* protonation is preferred in gas phase, imino-*N* protonation is preferred in polar condensed phase. While protonation is fast and exergonic in the gas phase, it is endergonic in polar condensed phase. It is an immediate consequence of these computational results that the direct observation of cations **9** and **10** is possible only in the gas phase.

In this context, it has been our aim to provide experimental evidence (1) for the existence of ions **8–10** and **12** and (2) for their formation by dediazoniation of the diazonium ions of the nucleobases **1h**, **2h**, and **3h**. With the present study, we address the first of these goals. The impetus for this study was provided by the realization that the ions produced by dediazoniation of the putative

Address reprint requests to Professor R. Glaser, Department of Chemistry, University of Missouri-Columbia, 321 Chemistry Building, Columbia, Missouri 65211,USA.E-mail: GlaserR@missouri.edu

1044-0305/07/$32.00
doi:10.1016/j.jasms.2007.08.018

Published online September 1, 2007
Received February 1, 2007
Revised August 28, 2007
Accepted August 28, 2007

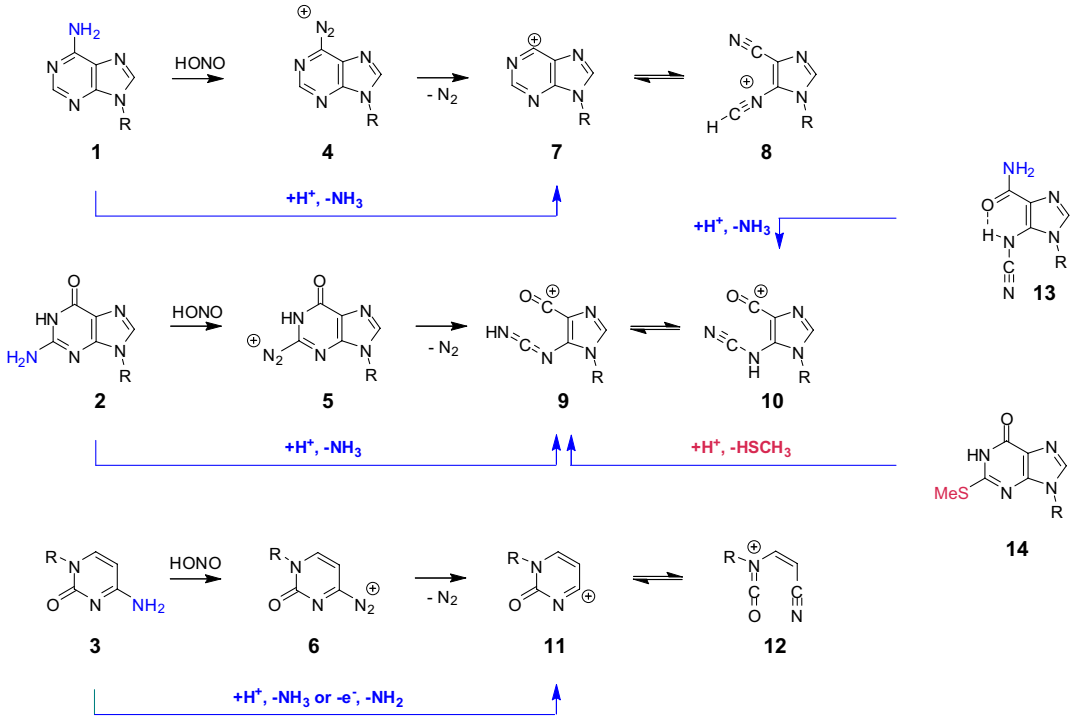

Scheme 1. Nucleoside and nucleobase deamination by nitrosation and by proton-catalyzed ammonia elimination.

nucleobase diazonium ions can be prepared in the gas phase via a sequence of protonation and ammonia elimination (Scheme 1). Hence, we have studied NH_3 elimination form the conjugate acids of the nucleobases **1h–3h** and the models **13h** and **14h**. We report the results of a gas-phase study of deamination of the protonated nucleosides adenosine **1r** (**1**, R = *r*ibose), guanosine **2r** (**2**, R = *r*ibose) and deoxycytidine **3d** (**3**, R = *d*eoxyribose). The study of the nucleosides is equivalent to the study of the nucleobases **1h–3h** because of the deglycation in the ESI experiments (vide infra) and the study of the nucleosides is advantageous because of their solubility. We also examined the potential formations of **9** and/or **10** from precursors **13e** (*e*ther R = $CH_2OCH_2CH_2OH$), 1-[(2-hydroxyethoxy)methyl]-5-cyanoamino-imidazole-4-carboxamide, and **14e**, 9-[(2-hydroxyethoxy)-methyl]-2-(methylthio)-hypoxanthine. The proton affinities of N-, O-, and S-sites were computed for aniline, for the nucleobases 9*H*-adenine, 1*H*,9*H*-guanine, and 1*H*-cytosine, for the (*Z*,*Z*)- and (*E*,*Z*)-rotamers of cyanoamine **13h** and for the (*Z*)- and (*E*)-rotamers of 2-thiomethyl-(1*H*,9*H*)-guanine **14h** (Scheme 2) to begin the discussion of the gas-phase ion chemistry. The formation of ammonium ions from the most stable protonated species has been studied by potential energy surface exploration and extensive reaction paths analyses have been performed. The MS analyses in

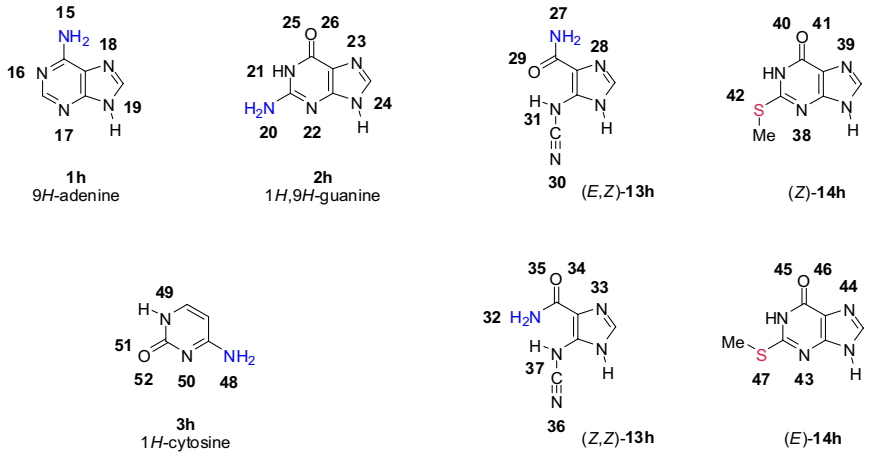

Scheme 2. Conjugate acids formed by protonation of **1h, 2h, 3h, 13h,** and **14h** are numbered according to the protonation sites as indicated.

Table 1. Voltages for in-source and in-collision cell CID

Analyte	Voltage: In-source CID	Voltage: Collision-cell CID	Figure
Adenosine, **1r**		40	1a
Guanosine, **2r**		30	1b
Deoxycytidine, **3d**		0	1c
[**1h** + H]$^+$, *m/z* 136	30	50	2a
[**8**]$^+$, *m/z* 119	30	35	2b
[**16**]$^+$, *m/z* 109	60	30	2c
[**2r** + H - 132]$^+$, *m/z* 152	20	50	3a
[**9**]$^+$, *m/z* 135	40	50	3b
[**25**]$^+$, *m/z* 110	50	50	3c
[**13r** + H]$^+$, *m/z* 226		20	4a
[**13h** + H]$^+$, *m/z* 152	30	5	4b
[**14r** + H]$^+$, *m/z* 257		35	4c
[**12h** + H]$^+$, *m/z* 112	30	50	5

conjunction with the computational assessment of pertinent gas-phase reactions provide compelling evidence for pyrimidine ring-opened species.

Experimental and Computational

Mass analyses were performed on a Thermo Finnigan TSQ7000 triple-quadrupole mass spectrometer (San Jose, CA) equipped with an AP12 source and Performance Pack. For all experiments, the heated capillary was maintained at 250 °C and the electrospray voltage was 4.5 kV. Voltages for in-source collision-induced dissociation and collision-induced dissociation [25] (CID) in the collision cell were optimized for each sample (Table 1). Other instrument parameters were optimized as part of bi-weekly maintenance and tuning. LC experiments employed a system that included a P4000 pump, AS3000 auto-sampler, and UV 6000 photodiode array detector.

For each of the three nucleosides, direct infusion MS experiments showed that the protonated nucleoside is the overwhelmingly dominant ion produced. In-source CID was used to promote deglycation of the nucleosides and to maximize the production of the corresponding protonated nucleobases. Parent ion scans for the protonated nucleobases produced by in-source CID demonstrate that they arise only from the corresponding nucleosides.

The nucleobases were further fragmented using CID in the collision cell of the mass spectrometer to yield the spectra shown. The overall information derived from the MS/MS experiments is equivalent to an MS/MS/MS experiment for each nucleoside. In some cases, in-source CID was used to deglycosylate the nucleoside and also fragment the nucleobase, giving access to ions further along some of the major degradation pathways and allowing positive identification of the fragments along those pathways.

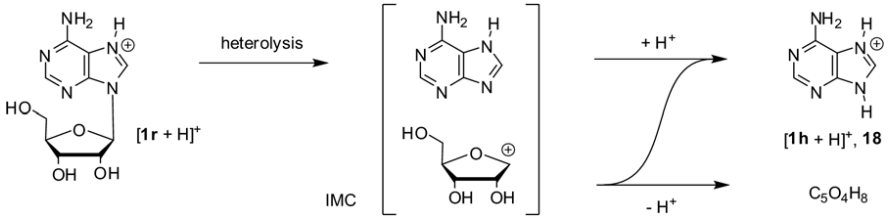

Scheme 3. Conversion of protonated nucleosides to protonated nucleobases.

Table 2. Calculated proton affinities of aniline, the nucleobases cytosine, adenine, and guanine, the (*E*,*Z*)- and (*Z*,*Z*)-rotamers of cyanoamine **13h**, and the (*Z*)- and (*E*)-rotamers of thioether **14h**[a]

Protonation site	Aniline	C	A	G	**13h** (*E*,*Z*)	**13h** (*Z*,*Z*)	**14h** (*Z*)	**14h** (*E*)
expt.	874[b]	976.4[c]	978.0[c]	981.4[c]				
NH_2	**879.9**	819.9	848.5	793.2	831.3	894.1		
N1		874.6[d]	**943.8**	813.6[d]				
N3		**955.4**	**937.5**	887.2			874.1	891.6
N7			909.9	**959.8**	876.2	**923.9**	**944.9**	**946.5**
N9			755.9	766.0				
C2−O, N1		921.6						
C2−O, N3		**956.9**						
C6−O, N1				900.7			895.9	890.2
C6−O, N7				**936.3**		914.4	927.7	925.1
C6−O, NH_2					868.0	872.2		
NCN, cyano					**924.5**	890.2		
NCN, amino					849.4	827.7		
S							760.7	

[a]Proton affinities (ΔH) in kJ/mol computed at B3LYP/6-31++G**. Data for guanine reported in reference [38]. Compare also [34, 36] for proton affinities of cytosine and adenine, respectively.
[b]Exp. value for aniline from references [42, 43].
[c]Exp. values for nucleobases from reference [40] (p. 9095).
[d]These protonated systems are ring-opened structures.

Table 3. Calculated relative energies and activation barriers[a]

Parameter	ΔE	ΔH_0	ΔH_{298}	ΔG_{298}
RE: Adenine **1h**				
E_{act}, **16** → **60**‡	203.72	191.07	189.86	191.74
E_{act}, **17** → **61**‡	175.40	164.26	162.42	164.50
E_{act}, **16** → **62**‡	279.83	263.29	266.26	259.51
E_{rel}, **63** *vs.* **16**	279.64	263.57	268.67	256.76
E_{act}, **63** → **64**‡	60.67	59.54	57.24	48.90
E_{rel}, **63** *vs.* **65**	60.42	59.75	59.55	58.97
RE: Guanine **2h**				
E_{act}, **23** → **74**‡	303.46	293.24	294.54	290.16
E_{rel}, **75** *vs.* **23**	131.27	119.88	123.81	112.97
E_{act}, **75** → **76**‡	32.02	30.85	29.43	32.15
E_{rel}, **77** *vs.* **75**	7.96	7.62	7.41	7.96
E_{act}, **77** → **78**‡	84.79	73.45	72.36	74.70
E_{rel}, **79** *vs.* **77**	39.14	39.10	39.81	38.51
E_{act}, **23** → **80**‡	268.54	251.04	251.29	249.31
E_{rel}, **81** *vs.* **23**	22.18	20.63	21.30	20.04
E_{act}, **81** → **82**‡	220.27	209.13	207.08	210.68
E_{rel}, **83** *vs.* **81**	126.85	128.98	128.36	129.01
E_{act}, **81** → **84**‡	235.28	224.23	222.30	225.54
E_{rel}, **85** *vs.* **81**	156.34	157.43	157.39	156.49
E_{act}, **23** → **86**‡	215.12	204.06	202.39	205.24
E_{rel}, **87** *vs.* **23**	124.47	126.56	126.73	124.12
E_{rel}, **22** *vs.* **23**	75.60	71.33	72.79	69.90
E_{rel}, **22** *vs.* **81**	53.41	50.69	51.49	49.85
E_{act}, **22** → **88**‡	243.33	232.11	230.19	233.57
E_{rel}, **89** *vs.* **22**	167.90	167.90	168.32	166.18
E_{act}, **22** → **91**‡	172.77	165.90	166.07	163.47
E_{rel}, **92** *vs.* **22**	150.79	148.36	148.48	144.88
E_{act}, **22** → **90**‡	195.97	185.88	183.28	187.95
E_{rel}, **20** *vs.* **22**	91.37	137.22	94.05	96.01
E_{rel}, **21** *vs.* **23**	152.19	142.68	146.45	136.28
E_{act}, **21** → **93**‡	239.08	225.89	224.97	224.73
E_{rel}, **94** *vs.* **21**	126.37	127.21	127.59	125.98
E_{act}, **95** → TS(**95**,**10′**)	194.02	178.41	162.71	164.25
RE: Model **13h**				
E_{rel}, **13h**, (*Z*,*Z*) *vs.* (*E*,*Z*)	60.55	60.42	60.42	60.07
E_{act}, **103** → **104**‡	50.06	44.66	39.34	38.30
E_{rel}, **105** *vs.* **103**	27.12	24.86	25.87	23.27
E_{act}, **105** → **106**‡	183.54	170.68	170.27	170.58
E_{rel}, **107** *vs.* **105**	38.57	38.91	39.49	37.68
E_{act}, **103** → **108**‡	77.23	76.06	74.72	76.71
E_{rel}, **109** *vs.* **103**	−0.92	−1.00	−0.88	−1.46
E_{act}, **109** → **110**‡	54.20	43.14	42.22	43.87
E_{rel}, **111** *vs.* **109**	1.84	1.38	1.92	0.51
E_{act}, **111** → **112**‡	44.76	43.51	42.04	44.76
E_{rel}, **113** *vs.* **111**	42.87	41.53	42.20	39.41
E_{act}, **113** → **114**‡	71.75	60.44	58.89	62.88
E_{rel}, **107** *vs.* **113**	21.91	21.86	22.12	22.49
E_{rel}, **118** *vs.* **107**	29.82	29.90	29.40	30.67
E_{rel}, **118** *vs.* **103**	95.51	93.67	94.76	91.63
E_{act}, **28** → **121**‡	95.40	85.52	83.59	89.47
E_{rel}, **27** *vs.* **28**	40.66	42.71	42.46	44.99
E_{act}, **33** → **122**‡	57.68	47.25	45.16	50.24
E_{rel}, **123** *vs.* **33**	41.50	42.68	41.71	45.00
E_{rel}, **28** *vs.* **103**	46.28	47.16	48.41	43.21
E_{rel}, **33** *vs.* **103**	57.84	60.22	61.02	58.11
E_{act}, **9** → TS(**9**,**125**)	294.63	289.27	286.34	294.88
RE: Model **14h**				
E_{act}, **39** → **128**‡	267.85	250.14	250.52	247.38
E_{rel}, (*Z*)-**129** *vs.* **39**	33.97	32.92	31.12	35.40
E_{act}, (*Z*)-**129** → **130**‡	15.22	15.14	13.13	17.96
E_{rel}, (*E*)-**129** *vs.* (*Z*)-**129**	−1.11	−1.24	−1.11	−1.74
E_{act}, (*Z*)-**129** → **131**‡	231.37	214.45	214.03	215.04
E_{rel}, (*E*)-**132** *vs.* (*Z*)-**129**	179.15	169.27	169.98	168.13
E_{act}, (*E*)-**129** → **133**‡	212.53	195.41	194.78	196.67
E_{rel}, (*E*)-**134** *vs.* (*E*)-**129**	171.44	161.69	162.19	159.80
E_{rel}, (*Z*)-**134** *vs.* (*E*)-**134**	15.04	14.37	14.70	12.75
E_{act}, (*Z*)-**39** → **135**‡	293.51	281.58	283.84	277.92
E_{rel}, **136** *vs.* (*Z*)-**39**	122.22	109.32	114.22	99.48
RE: Cytosine **3h**				
E_{act}, **50** → **138**‡	241.60	227.99	227.07	228.31
E_{rel}, **48** *vs.* **50**	141.80	141.38	142.09	139.41
E_{act}, **50** → **139**‡	364.07	349.34	352.02	343.21
E_{rel}, **140** *vs.* **50**	230.92	226.65	227.32	224.54
E_{act}, **50** → **141**‡	320.02	305.45	308.22	300.89
E_{rel}, **142** *vs.* **50**	77.96	70.38	74.27	64.24
E_{act}, **142** → **143**‡	240.50	227.31	226.35	227.31
E_{rel}, **144** *vs.* **142**	143.76	143.76	144.17	142.05
E_{act}, **50** → **145**‡	341.93	327.70	315.89	310.08
E_{rel}, **146** *vs.* **50**	87.79	80.76	77.87	67.13

[a]All data in kJ/mol and determined at B3LYP/6-31++G**.

Adenosine, guanosine, and deoxycytidine were purchased from Sigma (St. Louis, MO) and used without further purification. Samples were prepared by dissolving 1 mg nucleoside in 1 mL of 1% acetic acid solution. The preparations of the cyanoamine **13** and the thioether **14** have been described previously [21]. The LC-MS studies were performed with a Waters XTerra analytical column (C18, 5 μm, 4.5 × 250 mm, Milford, MA) using a solvent gradient (Solvents A and B are 0.1% formic acid and acetonitrile, 1% B at 1 min, 10% B at 3 min, 40% B at 20 min, 1% B at 22 min) at a flow rate of 1.0 mL/min while monitoring at $\lambda = 254$ nm.

The structures of the nucleobases and the models of their conjugate acids, and of various intermediates and transition states along relevant reaction paths were determined with density functional theory (DFT) [26]. The hybrid method B3LYP was employed in conjunction with the 6-31++G** basis set, B3LYP/6-31++G**, and the calculations were performed with Gaussian03 [27] on a 64-processer SGI Altix system (Sunnyvale, CA). Structures were optimized and vibrational analysis was performed for each structure to confirm that the structure was in fact stationary, to confirm the character of the stationary structure, and to determine thermochemical data. Total energies E, vibrational zero-point energies $VZPE$, thermal energies TE, and entropies S are tabulated in Supplementary Material section, which can be found in the electronic version of this article, and Cartesian coordinates of all optimized structures are provided there as well. These data allow for the determination of relative and reaction energies ΔE, enthalpies $\Delta H_0 = \Delta(E + VZPE)$ and $\Delta H_{298} = \Delta(E + TE)$, and free energies $\Delta G = \Delta(E + TE - 298.15 \cdot S)$. Unless otherwise noted, we report ΔH_{298} values in kJ/mol, Table 2 provides for an overview of proton affinities, and in Table 3 are listed relevant relative and activation energies.

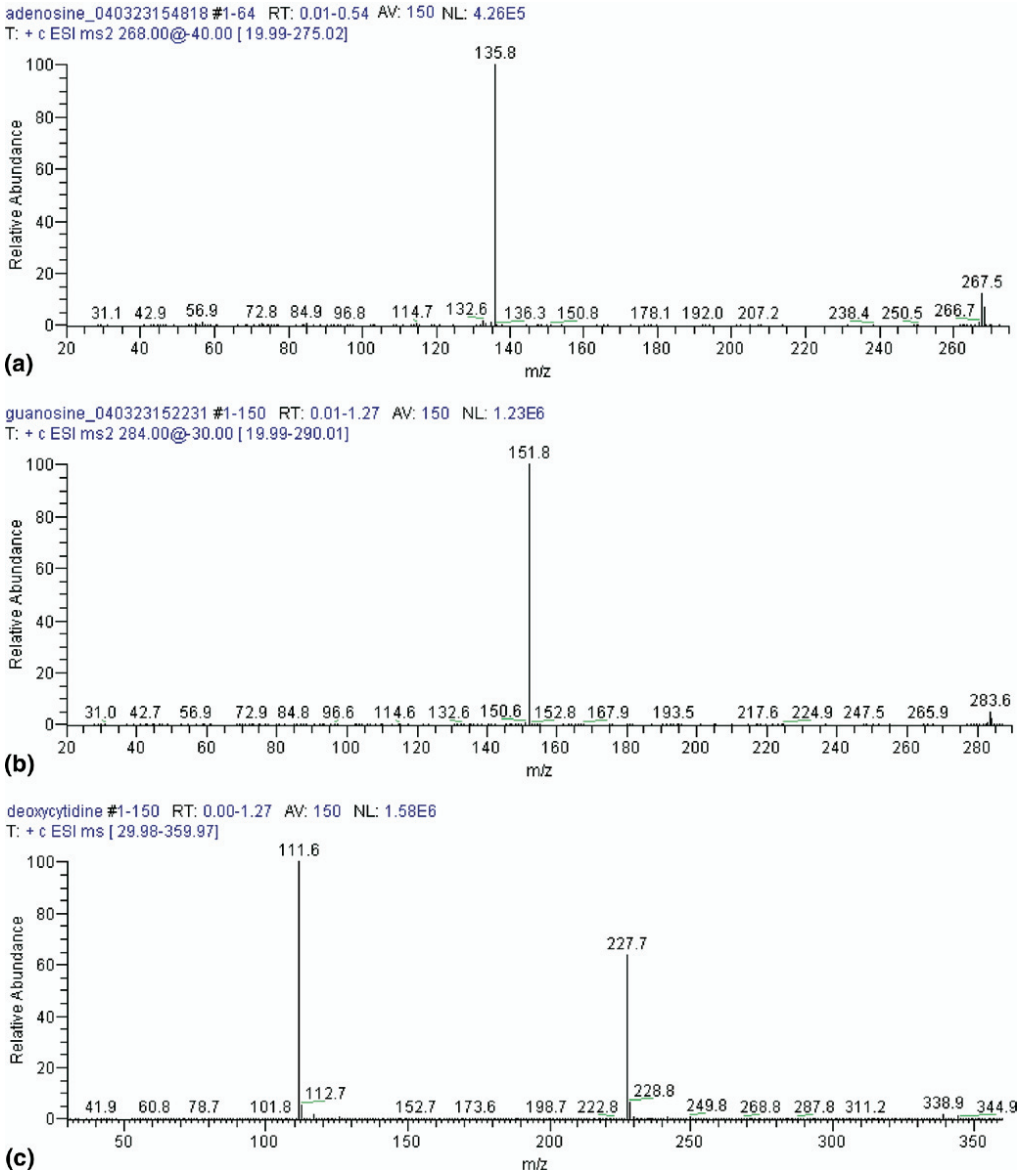

Figure 1. Product-ion spectra of (**a**) protonated adenosine [**1r** + H]$^+$, *m/z* 268, and (**b**) protonated guanosine [**2r** + H]$^+$, *m/z* 284. (**c**) The mass spectrum of deoxycytidine features [**3d** + H]$^+$, *m/z* 228, and [**3h** + H]$^+$, *m/z* 112.

Results and Discussion

Initial Expulsion of Nitrile or Ammonia

The mass spectra of the nucleobases have been studied using electron-impact ionization many years ago [28]. The EI study of adenine showed that the major fragmentation path involves successive loss of HCN molecules. Studies of labeled adenines [29, 30] demonstrated that the initially eliminated HCN contains the N1 atom and the loss of the NH_2 group was *not* observed. For guanine, the initial expulsion of neutral cyanamide (H_2NCN) is the dominant fragmentation (from the pyrimidine's N1-C2-NH_2 moiety), and some NH_2 group elimination was observed as well. For cytosine [31], NH_2 elimination was observed and it is followed by loss of HCN. Initial decarbonylation of the molecular ion also was observed, and the peaks at *m/z* 69, 68, and 67 were explained by retro-Diels-Alder reactions eliminating first ·*N*=C=O, HNCO, or H and HNCO, respectively, and subsequent HCN loss. Alternatively, the *m/z* 95 peak might be due to **11h** (**11**, R=H) as well as **12h**, and the peak *m/z* 68 could be explained as the result of elimination of HCN or HNC from **12h** and the formation of protonated isocyanatoethyne. Hence, the observation of *m/z* 68 might present a first indication for the possible existence of **12**.

ESI and Deglycation

Electrospray ionization (ESI) mass spectrometry of the nucleosides is employed in the diagnosis of purine and pyrimidine metabolic disorders. Fryèák et al. [32] reported that the dominant fragmentation of the nucleoside molec-

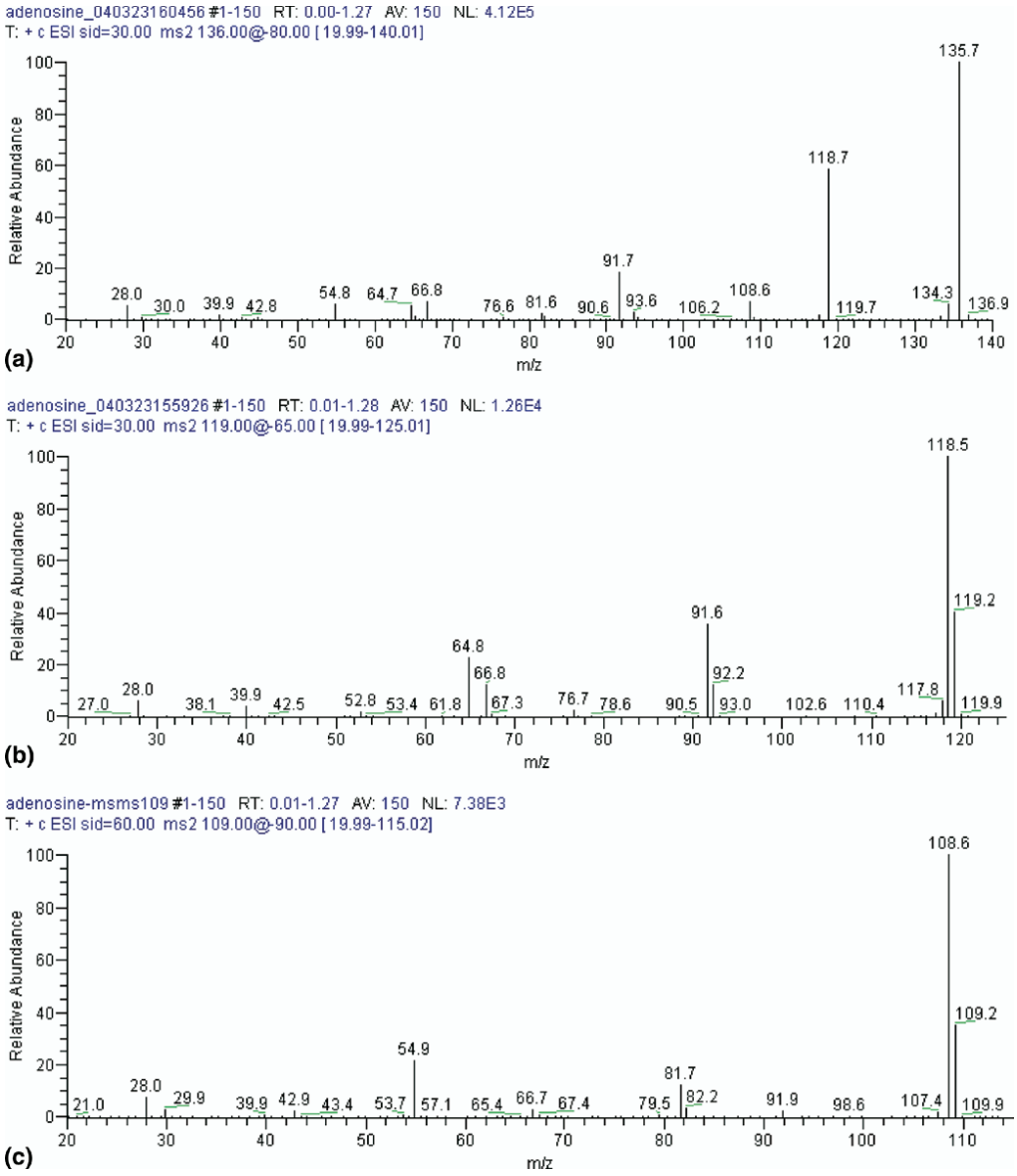

Figure 2. Product-ion spectra of (**a**) [**1h** + H]$^+$, *m/z* 136, (**b**) **8′**, *m/z* 119, and (**c**) **16**, *m/z* 109. All of these precursor ions were produced by in-source fragmentation of [**1r** + H]$^+$ at increasing energies.

ular ions is the collision-induced dissociation of the glycosidic C–N bonds and leads to the replacement of the sugar moiety by a hydrogen atom, as had been suggested by McCloskey [33a]. The process is shown in Scheme 3 for the conversion of adenosine **1r** (**1**, R = ribose) to adenine **1h** (**1**, R=H) and assuming N7-protonation [32]. The resulting ion forms an ion-molecule complex (IMC) by heterolysis of the glycosidic C-N bond and the intermittent neutral purine is protonated by the oxocarbenium sugar moiety. The spectra in Figure 1 demonstrate these deglycation reactions for **1r**, **2r**, and **3d**. McCloskey et al. studied the CID spectra of protonated adenine [33b] and protonated guanine [33c]. More recently, Tureček et al. [34] and Wang et al. [35] reported on their experimental and computational studies of protonated cytosine, Tureček et al. [36] explored the dissociation mechanisms of protonated adenine in detail, and we will refer to these reports in the Discussion.

Site of Protonation and Mode of Initial Fragmentation

The computed proton affinities (Table 2) show that the theoretical level employed presents an acceptable compromise between desired accuracy and computational demand [37]; the computed proton affinities are within 5% of the experimental values.

There is general agreement with earlier theoretical studies of the purine bases [36–40] and of cytosine [34, 41]. The measured proton affinity of aniline is 874 kJ/mol (208.8 [42] and 209.5 kcal/mol [43])and experimental [44] and theoretical [45] studies showed almost equal propensity for protonation at the amino-N- and the *para*-C-atoms. The proton affinities of the amino group of the nucleobases are lower than for aniline and, moreover, amino group protonation cannot compete with the alternatives (Table 2). Guanine prefers imidazole ring protonation

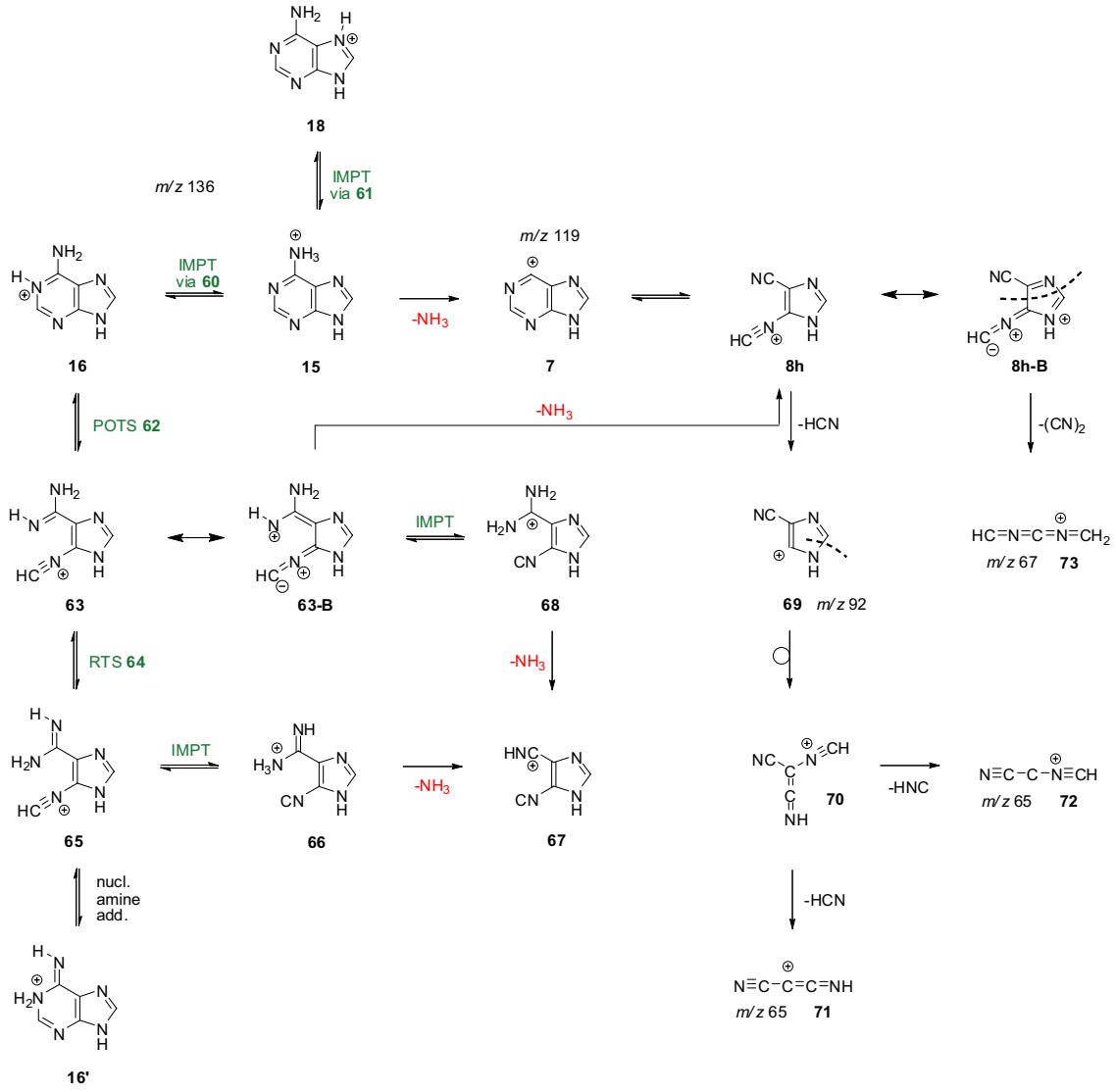

Scheme 4. Fragmentation paths of protonated adenine beginning with NH_3 elimination.

with carbonyl-O protonation being a close second, adenine prefers pyrimidine ring protonations, and for cytosine the proton affinities for N3- and O-protonation are similar.

The amino group is *not* the best protonation site for the nucleobases and the model systems, and we have to discuss how the amino group can serve as the dissociative protonation site [46] or consider alternative mechanisms for ammonia elimination. Some guidance is provided by the emerging understanding of NH_3 elimination from peptides [47]. The "mobile proton model" holds that intramolecular proton migration to various protonation sites can occur before fragmentation. In cases with impediments to proton mobility [48], the ammonia elimination might occur as the result of complex mechanisms [49, 50]. Hence, the potential energy surfaces of the protonated systems were explored to search for and to determine the energy profiles of paths for proton migration leading to the formation of ammonium ions.

ESI-MS/MS of Adenosine

The mass spectrum of electrosprayed adenosine gave two peaks as shown in Figure 1. *m/z* 268 [**1r** + H]$^+$ is protonated adenosine and *m/z* 136 [**1h** + H]$^+$ results by cleavage of the glycosidic C–N bond. Mass selection for *m/z* 136 and application of CID results in the spectrum of Figure 2, the mechanisms of the fragmentation of the quasimolecular ion *m/z* 136 are outlined in Scheme 4, and molecular models of relevant intermediates and transition-state structures are shown in Scheme 5.

The minor paths for fragmentation of ion [**1h** + H]$^+$ involve initial loss of HCN or NH_2CN and these are the fragmentations observed in EI-MS. The MS/MS analysis of ion **53** (Figure 2c) shows the formations of ions **54** (*m/z* 82) and **55** (*m/z* 55) by successive losses of three HCN and resulting in the formation of **56** (*m/z* 28), protonated HCN. Initial elimination of cyanoamine leads to **57** (*m/z* 94) and

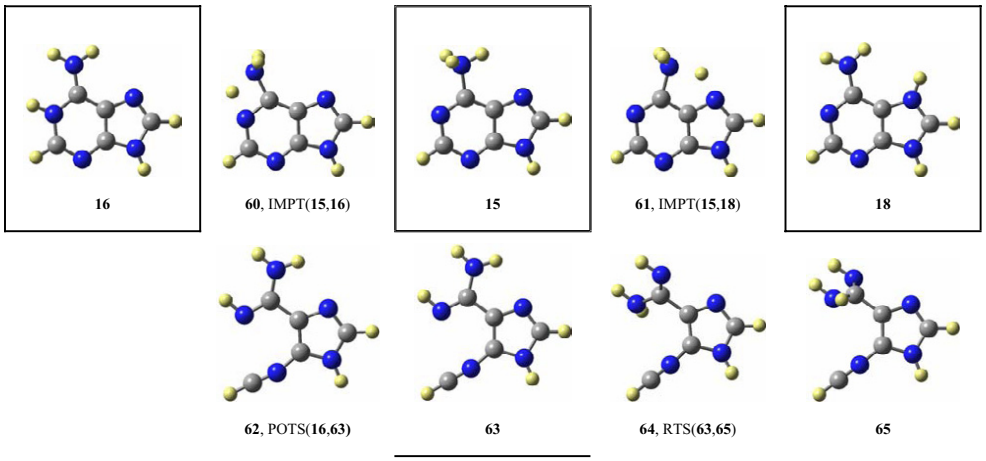

Scheme 5. Intramolecular proton transfer allows for the conversions of N1- and N7-protonated tautomer **16** and **18** (bold single-lined boxes) to the ammonium tautomer **15** (double-lined). Pyrimidine ring-opening of N1-protonated adenine may lead to amidines **63** and **65** but these paths are not competitive.

another HCN (or HNC) elimination cascade from **57** to **58** (*m/z* 67) to **59** (*m/z* 40).

Amino protonation is less likely than protonation at N1, N3, or N7 of adenine **1h** (Table 2) and ammonium ion **15** would have to be generated by proton migration within $[\mathbf{1h} + H]^+$. Proton transfers from **16** and **18** to **15** via transition-state Structure **60** and Structure **61**, respectively, require activation enthalpies of 189.9 and 162.4 kJ/mol, respectively.

One can also envision the formation of **8h** by direct NH_3 elimination from **63** (consider resonance form **63-B**) via **68** or from **65** via **67** if **65** does not reclose to **16′** [51]. These options depend on the accessibilities of **63** and **65**. Indeed, **63** and **65** are minima on the potential energy surface, **63** is preferred over **65** by $\Delta E = 60.4$ kJ/mol, and the rotational barrier for the conversion of **63** to **65** via transition-state structure **64** is $\Delta E = 60.7$ kJ/mol. With thermal energies considered, this activation barrier vanishes, and **65** becomes the transition-state structure for the rotational automerization of **63** with an activation enthalpy of $\Delta H_{298} = 59.6$ kJ/mol. There is hardly any barrier to the back-reaction of **63** via transition-state structure **62** to **16**, this feature is the hallmark of pseudopericyclic reactions [52], and the relative energy of **63** with regard to **16** is 268.7 kJ/mol. Tureček et al. [36] showed that **63** plays a crucial role to exchange the N1- and the amino-N atoms in $[\mathbf{1h} + H]^+$.

The major fragmentation cascade of $[\mathbf{1h} + H]^+$ begins with NH_3 elimination from **15** or **63** to yield **8h** with *m/z* 119 (Figure 2a). The subsequent HCN (or HNC) elimination can be explained conveniently from **8h**. Ion **69** then can rearrange to **70** on its way to ions *m/z* 65, protonated dicyanocarbene **71** and/or its mono-isonitrile isomer **72** (Figure 2b).

We found that ion *m/z* 119 also leads to fragments *m/z* 67 and *m/z* 40 (Figure 2b). The $H_3C_3N_2^+$ ion occurs as **58** in the decomposition path initiated by NH_2CN elimination and an ion with this formula also can form along the major path. Considering resonance form **8h-B** we propose that *m/z* 67 might result by dicyanogen (ethanedinitrile) elimination to form the protonated cumulene **73**.

ESI-MS of Guanosine

The mass spectrum of electrosprayed guanosine gave a product peak at *m/z* 152 after cleavage of the glycosidic CN bond (Figure 1). Figure 3 shows the product-ion spectra obtained by CID of $[\mathbf{2h} + H]^+$, *m/z* 152, and its two most abundant fragments *m/z* 135 and *m/z* 110 resulting from NH_3 and cyanamide elimination. We considered seven paths, which are shown in Scheme 6; relevant stationary structures are shown in Scheme 7.

The N7-protonated tautomer **23** is the most stable and most abundant ion of $[\mathbf{2h} + H]^+$. We first considered the pyrimidine ring-opening of **23** to **74** by a pseudopericyclic reaction mechanism. We found that an amidine with a **74**-like structure does not correspond to a minimum and, instead, rotation about the C2–N3 bond via transition-state structure **74** results in amino-group transfer along the down path from **74** to **75**. The computed activation barrier for the reaction **23** → **74**‡ → **75** is $\Delta H_{298} = 294.5$ kJ/mol and, should **75** be accessible, one could envision the facile formation of **9′** via **77** and **79**. Next, we considered two paths that begin with initial proton migration to **81**; the computed activation barrier for the reaction **23** → **80**‡ → **81** is $\Delta H_{act} = 251.3$ kJ/mol; some 40 kJ/mol lower than the path via **74**. The back-reaction of **81** is less likely than the intramolecular proton transfers **81** → **82**‡ → **83** ($\Delta H_{act} = 207.1$ kJ/mol) and **81** → **84**‡ → **85** ($\Delta H_{act} = 222.3$ kJ/mol). Ammonium ions **83** and **85** are substrates for the formations of **9′** and **10′**.

The initial proton transfer **23** → **81** was considered because we thought that NH_3 elimination required electrophilic catalysis, that is, the availability of an acidic H atom for 1,2-elimination. Eventually, we came to wonder whether the N1-hydrogen in **23** might not be acidic enough for the reaction **23** → **86**‡ → **87**. In fact, the nonstandard resonance form **23-C** makes perfect sense:

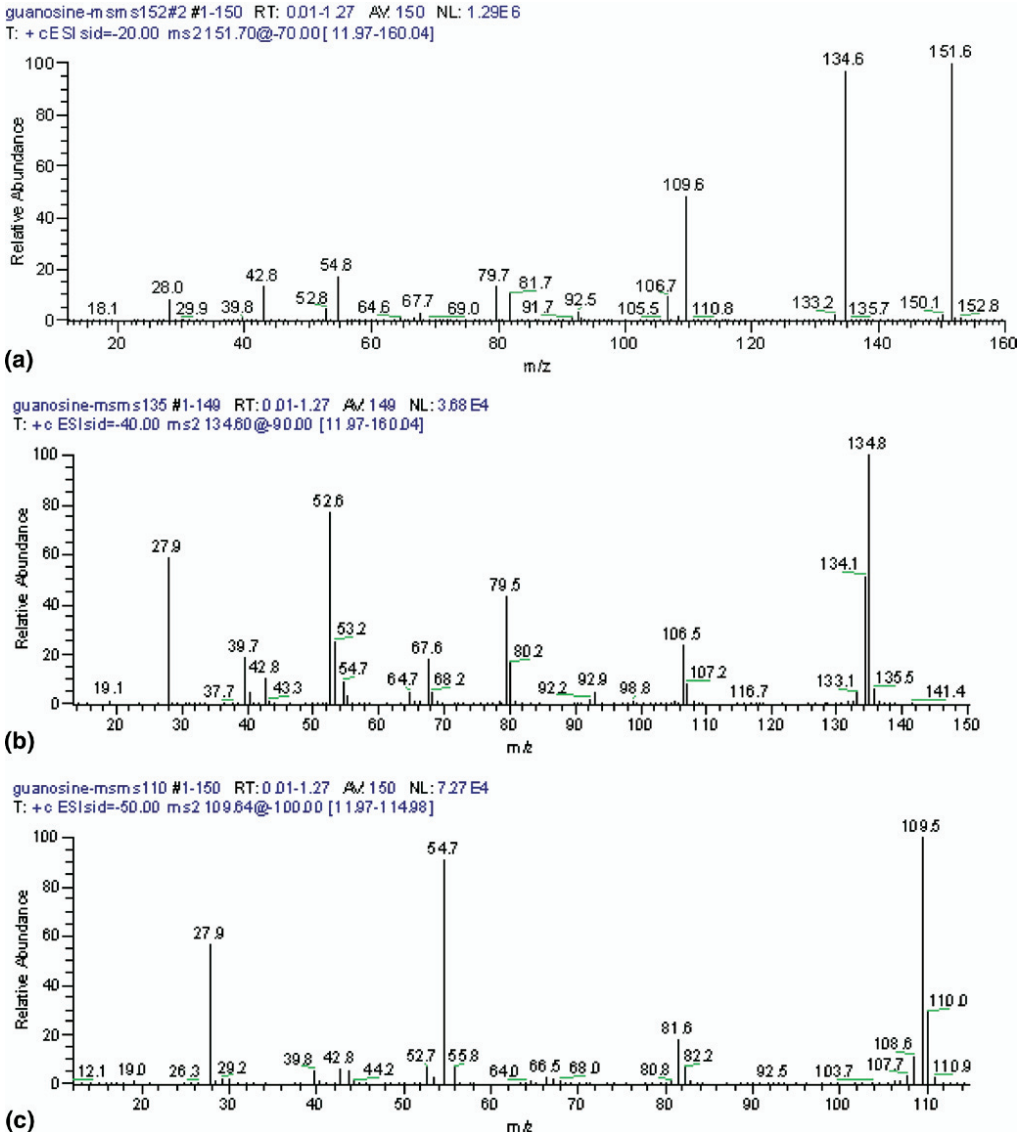

Figure 3. Product-ion spectra of (**a**) [**2h** + H]$^+$, *m/z* 152, (**b**) **9′**, *m/z* 135, and (**c**) **98**, *m/z* 110. All precursors were produced by in-source fragmentation of [**2r** + H]$^+$ at increasing energies.

the zwitterion-like π-polarization is effective to stabilize the charge in the σ-system caused by N7-protonation. Indeed, reaction **23** → **86**‡ → **87** requires an activation barrier of only ΔH_{act} = 202.4 kJ/mol.

Ion **23** is the most stable tautomer of [**2h** + H]$^+$ and it can be formed directly from [**2r** + H]$^+$. The initial formations of tautomers **21** and **22** are possible and their isomerizations to **23** should be fast in the hot ion [**2h** + H]$^+$. Nevertheless, the isomerizations **23** → **20**, **23** → **21**, and **23** → **22** could be relevant for the fragmentation. The conversion of **23** to **20** likely would proceed via **81** and **22** in that sequence. Nevertheless, suppose that **22** were accessible from **23** without going through **81**, such a path **23** → **22** would become interesting only if **22** were to offer a reaction channel for NH_3 elimination with a barrier that was at least 72.8 kJ/mol lower than for the reaction **23** → **87**. The conversion of **23** to **21** is likely to proceed via **26** and **25**. Since **21** is 146.5 kJ/mol less stable than **23**, the path **23** → **21** becomes interesting if **21** were to offer any reaction channel for NH_3 elimination with a barrier that were at least that much lower than for the reaction **23** → **87**. Neither of these options seemed likely, but they were explored to be sure and we computed the reactions **22** → **88**‡ → **89** (ΔH_{act} = 230.2 kJ/mol), **22** → **90**‡ → **20** (ΔH_{act} = 183.3 kJ/mol), **22** → **91**‡ → **92** (ΔH_{act} = 166.1 kJ/mol), and **21** → **93**‡ → **94** (ΔH_{act} = 225.7 kJ/mol). The situations with **22** → **91**‡ → **92** and **23** → **74**‡ → **75** allow for an interesting comparison and an acyclic amidine does not exist in either case. Hence, there are two paths from **22** and one path from **21** to ammonium ions, and the computed activation barriers show that these paths do not offer alternative, low-energy channels.

These results suggest that the reaction **23** → **86**‡ → **87** with its activation barrier of ΔH_{act} = 202.4 kJ/mol provides the most easily accessible channel to an ammonium ion of [**2h** + H]$^+$, and that NH_3 elimination yields **95**, a

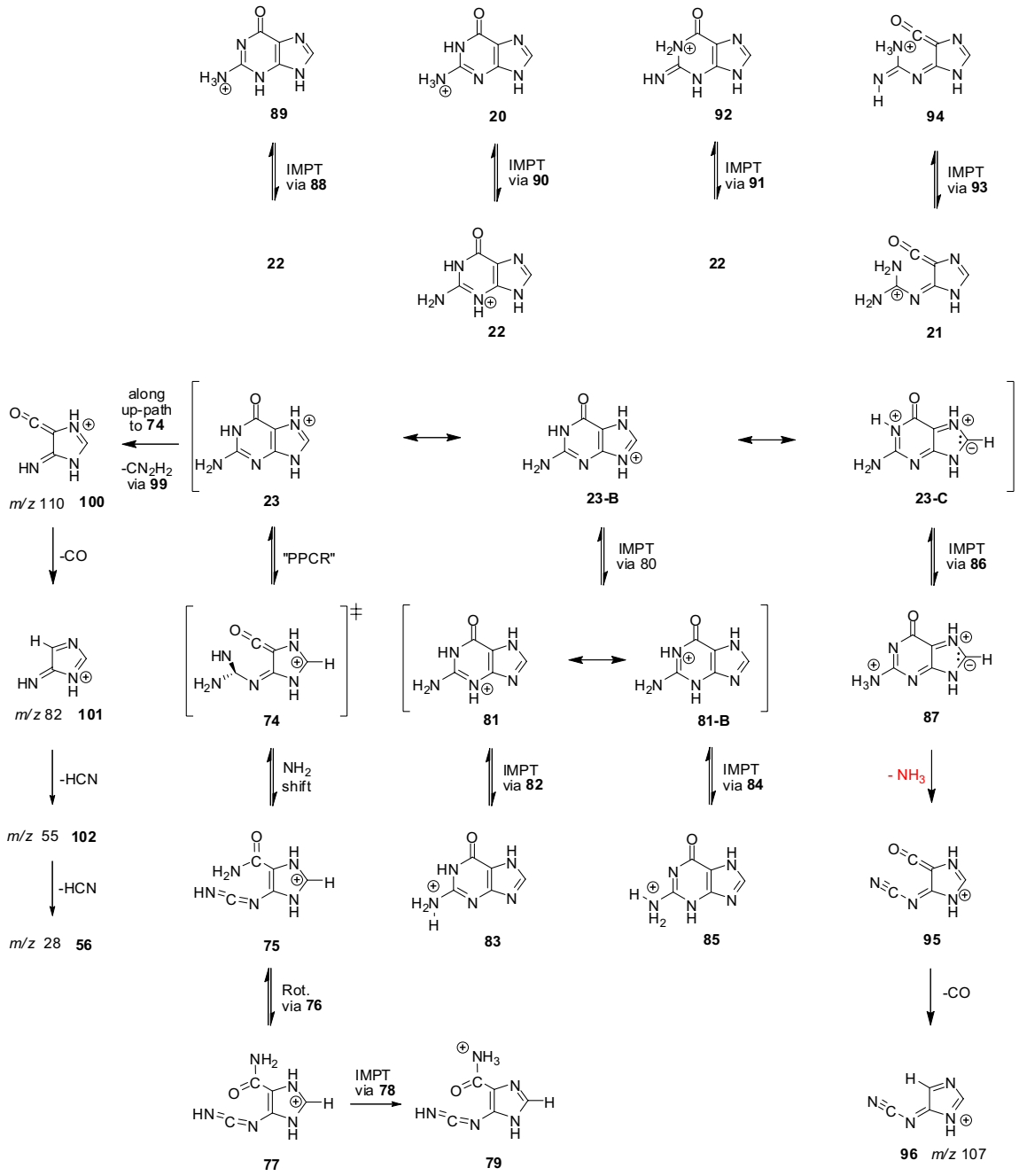

Scheme 6. Fragmentation paths of protonated guanine [**2h** + H]$^+$.

tautomer of carbodiimides **9** and **9′** and of cyanoimines **10** and **10′**. In the gas phase, the activation barrier for the isomerization between the prototypical carbodiimide and cyanamide is over 330 kJ/mol [53]. The tautomerization of **95** to **10′** requires an activation enthalpy of ΔH_{act} = 162.71 kJ/mol but even this low barrier apparently does not allow for competition with decarbonylation and 1,2-H-shift to **96** (*m/z* 107). The loss of CO requires the proximity of an NH site so that the incipient carbene can be stabilized [54]. HCN loss from ion *m/z* 107 results in **97** (*m/z* 80), and **97** can loose another HCN (or HNC) to form **98** (*m/z* 53, $C_2N_2H^+$) or eliminate dicyanogen to form **56** (*m/z* 28, H_2CN^+).

Initial cyanamide expulsion is the dominant mode of guanosine decomposition in EI-MS, the process leads to the *m/z* 110 ion, and its product-ion spectrum is shown in Figure 3c. It appears likely that **23** itself is the most suitable precursor for the NH_2CN elimination. The stage is set for CN_2H_2 elimination as soon as the N1–C6 bond of **23** is mostly broken along the up-path to transition-state structure **74**. There are many options to accomplish the tasks of second CN cleavage and proton transfer (from NH or NH_2 to O or N), these elemental reactions could occur within ranges of the up-path to the rotational transition-state region, and these tasks might occur stepwise or in concert. The PES exploration of reaction **23** → **74**‡ → **75**

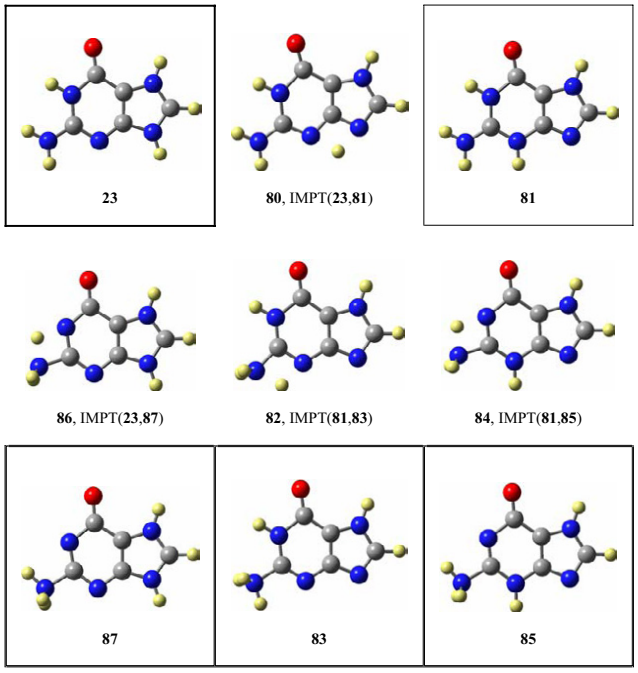

Scheme 7. N7-Protonated guanine **23** (bold single-lined) is the most stable structure of [**2h** + H]$^+$. The paths are shown for the formations of ammonium ion precursor **81** (single-lined) and of their ammonium ions **83, 85,** and **87** (double-lined).

suggests, for example, that one amino-H in a **74**-like structure would be well-positioned to transfer to N3, that is, for carbodiimide elimination via transition-state structure **99** and leading directly to **100** (Scheme 6). The prominent peaks with *m/z* values of 82, 55, and 28 further suggest decarbonylation to **101**, and HCN (or HNC) eliminations to **102** and **56**. The possibility of proton transfer to O along the up-path to **74** cannot be dismissed in and of itself; such a course of reaction would make the CO elimination a complicated affair but not an impossible one.

*ESI-MS Spectrometry of 5-Cyanoamino-Imidazole-4-Carboxamide **13e***

We synthesized cyanoamine **13e** (**13**, *e*ther R = $CH_2OCH_2CH_2OH$) and studied its cyclization reaction and cross-link formation chemistry [21, 22]. The product-ion spectra of [**13e** + H]$^+$, *m/z* 226, and [**13h** + H]$^+$, *m/z* 152, are reported in Figure 4. As with Figure 1, the spectrum in Figure 4a shows the replacement of the R-group by an H-atom to form [**13h** + H]$^+$, *m/z* 152.

Ion [**13h** + H]$^+$ eliminates ammonia as in the case of [**2h** + H]$^+$. However, [**13h** + H − NH_3]$^+$ does *not decarbonylate* subsequently and instead loses CN to form *m/z* 109. The potential energy surfaces of **13** and [**13** + H]$^+$ are complex because of the possibility for rotamers (about both exocyclic bonds) and tautomerism (cyanoamine versus carbodiimide) and a complete discussion will be presented elsewhere while some relevant data are included here. For the present purpose it is important to know that (*E,Z*)-**13h** is preferred over any of the carbodiimides and also preferred by ΔH_{rel} = 60.3 kJ/mol over (*Z,Z*)-**13h**. Studies of amides suggest that NH_3 elimination occurs only from the ammonium ion [55]. Yet, neither carbonyl-O nor amino-N protonation can compete with nitrilium or imidazolium ion formation (Table 2). Hence, we considered paths to ammonium ion formation from nitrilium and imidazolium ions (Scheme 8).

Cyano-*N* protonation is by far the best option for cyanoamine (*E,Z*)-**13h** and ion **9** becomes accessible by NH_3 elimination from ammonium ion **107**. Cyano-*N* protonation of (*E, Z*)-**13h** does not form a stable nitrilium ion **30** and O-protonated carbodiimide **103** is formed instead. Its rotamer **105** is easily accessible via rotational transition-state structure **104** (ΔH_{act} = 39.3 kJ/mol) but proton migration (from the OH-donor) **105** → **106**‡ → **107** requires an activation energy of ΔH_{act} = 170.3 kJ/mol. Another path from **103** to **107** via **109** and **111** involves a series of rotations and offers the advantage of forming the ammonium ion by H-shift from the NH-donor **113** with a barrier of only ΔH_{act} = 58.9 kJ/mol. The highest rotational barrier along this path is ΔH_{act} = 74.7 kJ/mol for the isomerization **103** → **108**‡ → **109** (and this isomerization could be accomplished in three steps with lower activation barriers via intermediates **105** and **116**). There are many paths from **103** to **107** and clearly at least some of them are kinetically facile.

As with the formation of **103** from (*E,Z*)-**13h**, ion **118** would be easily available by cyano-N protonation of (*Z,Z*)-**13h**. In the absence of (*Z,Z*)-**13h**, however, **118** would have to be produced from **116** by H-shift via **120** or by isomerization of **107** via rotational transition-state structure **119**. At least the latter path is accessible but none of this matters anyhow because **118** is less stable than **107** by ΔH_{rel} = 29.4 kJ/mol.

The direct formation of **28** by N7-protonation of (*E,Z*)-**13h** would offer the advantage to make ammonium ion **27** accessible via transition-state structure **121** with activation energy ΔH_{act} = 83.6 kJ/mol. Direct protonation of (*Z,Z*)-**13h** favors the formation of imidazolium ion **33** (Table 2) and ammonium ion **123** is then accessible by the H-shift **33** → **122**‡ → **123** with an activation energy of only ΔH_{act} = 41.7 kJ/mol. Yet, in the MS experiment, **28** and **33** have to be formed from **103** and these ions are 48.4 and 61.0 kJ/mol less stable, respectively, than **103**. These relative energies together with the computed barriers to form **27** and **123** show that there are no low-energy alternatives to the formation of ammonium ion **107**.

The potential energy surface of protonated 5-cyano-imino-4-oxomethylene-dihydroimidazole is complicated [24] and we have already seen that it includes rotamers of **9** and **9′**, rotamers of **10** and **10′**, and rotamers of **95**. In addition, geometrical isomers of O-protonated species also are possible, and it becomes relevant that O-protonation leads to bicyclic ions **125** and **125′**. Cation **9** prefers the *E*-conformation about the C–(N_2CH) bond and the equilibration (*Z*)-**9** ⇄ (*E*)-**9** is facile [19]. The intramolecular H-shift from nitrogen in (*E*)-**9** to the oxygen in **125** requires an activation energy of ΔH_{act} = 268.3 kJ/mol and the accessibility of **125**

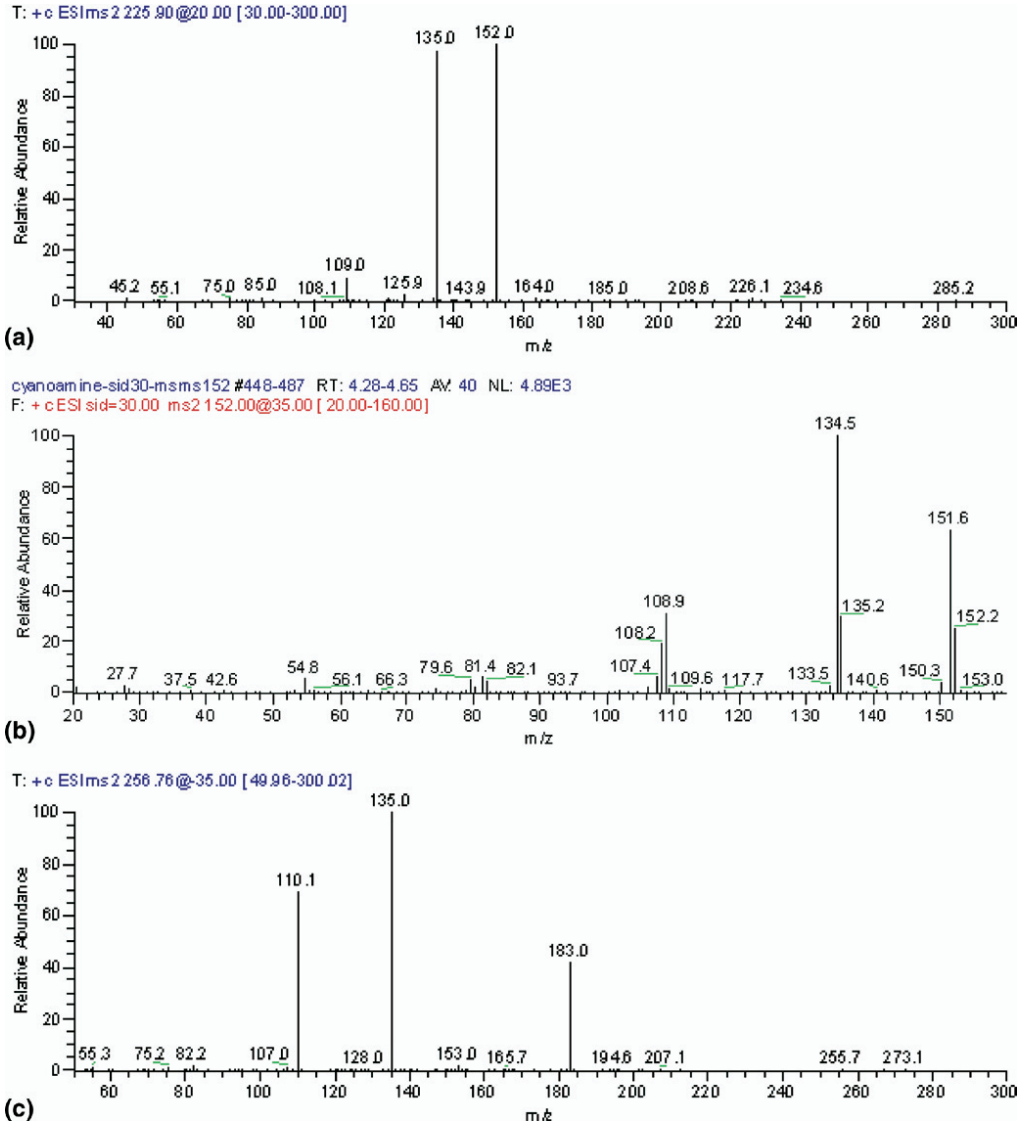

Figure 4. (**a**) Product-ion spectrum of [**13r** + H]$^+$, *m/z* 226. (**b**) Product-ion spectrum of [**13h** + H]$^+$, *m/z* 152, produced by in-source fragmentation of [**13r** + H]$^+$. (**c**) Product-ion spectrum of [**14r** + H]$^+$, *m/z* 257.

provides a rational for CN elimination from **9** and leading to **126**.

ESI-MS Spectrometry of 2-Methylthiohypoxanthine 14h

Thioether **14e** (**14**, with *e*ther R = $CH_2OCH_2CH_2OH$) is a side-product in the synthesis of cyanoamine **13e** and presents as a possible precursor for ions **9** and **10**. The product-ion spectrum of [**14h** + H]$^+$ shown in Figure 4 is similar to that of the respective guanosine analog [**2h** + H]$^+$ of Figure 3; its fragmentation is described in Scheme 9 and relevant stationary structures are shown in Scheme 10.

The proton affinities of H_2S and MeSH are 744.8±10.0 kJ/mol [56] and 774.0 ± 4.2 kJ/mol [57], respectively. The computed affinities for S-protonation of **14h** fall into this range (Table 2). As with guanine, N7-protonation is preferred and we discuss the fragmentation options of the N7-protonated ion **39** of [**14h** + H]$^+$. The major characteristics of the fragmentation of [**14h** + H]$^+$ and [**2h** + H]$^+$ are analogous.

The initially formed ion **39** occurs in the (*Z*)-conformation only and its conversion to (*Z*)-**129** via transition-state structure **128** requires ΔH_{act} = 250.5 kJ/mol. Once (*Z*)-**129** is reached, its slightly more stable rotamer (*Z*)-**129** also is easily accessible via rotational transition-state structure **130**. The reaction (*E*)-**129** → **133**‡ → (*E*)-**134** requires an activation barrier of ΔH_{act} = 194.8 kJ/mol and (*Z*)-**134** then becomes accessible by facile S-inversion. In the case of **132**, (*E*)-**132** is the only existing rotamer and it is formed by the reaction (*Z*)-**129** → **131**‡ → (*E*)-**132** with an activation barrier of ΔH_{act} = 214.0 kJ/mol.

As with protonated guanine, we explored whether a ring-opened structure of type **135** might exist as a minimum, and it was found that such a structure

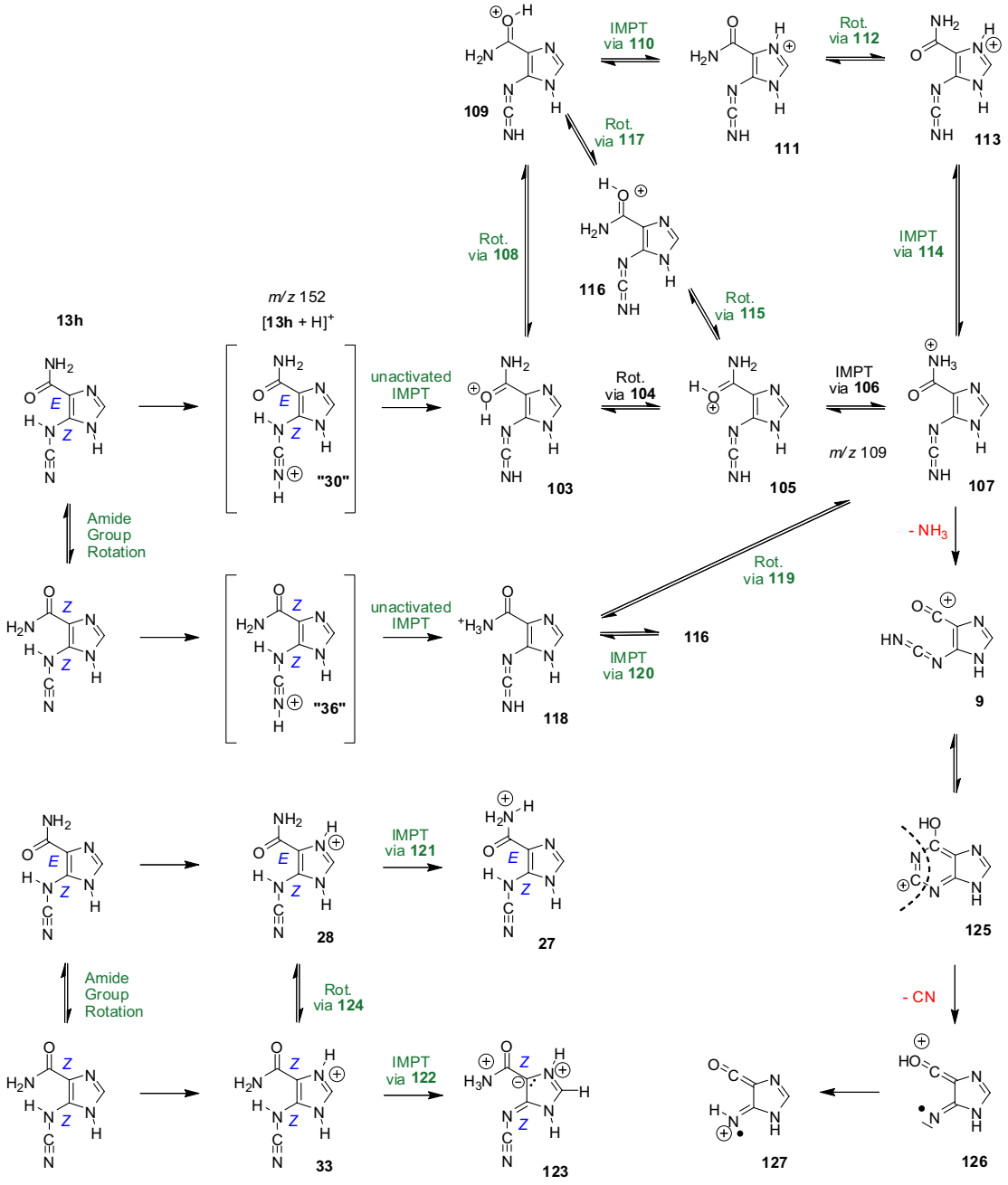

Scheme 8. Fragmentation of protonated 5-cyanoaminoimidazole-4-carboxamide [**13h** + H]$^+$.

serves as the transition-state structure for the formation of **136**. The ascent to **135** requires ΔH_{act} = 283.8 kJ/mol and significantly more activation than the formation of **129**. It remains to be explored whether the PES region along the up-path to **135** offers entry points for methyl isothiocyanate expulsion. The above discussion of carbodiimide elimination from protonated guanine via transition-state structure **99** and leading to **100** (Scheme 6) applies in complete analogy to the formation of **100** via **137**.

The computational analysis suggests that **134** is the precursor for MeSH elimination and, hence, ion [**14h** + H − MeSH]$^+$ most likely leads to structure **9′** via the least-energy path. Yet, structure **10′** cannot be dismissed because every (*Z*)-**129** formed contains enough energy to overcome any of the barriers along the paths to **9′** or **10′**.

The discussions of the fragmentations of [**2h** + H]$^+$ and [**13h** + H]$^+$ (Schemes 6 and 8) suggest that the preference of [**2h** + H]$^+$ for CO elimination from **95** and the preference of [**13h** + H]$^+$ for CN elimination from **9** are consequences of the hydrogen pattern. The absence of CO loss in the fragmentation of [**14h** + H]$^+$ shows that an NH in the proximity of the putative carbene site is not sufficient to enable decarbonylation. Decarbonylation only occurs from **95**, the ion in which the proximate NH is part of the imidazolium system.

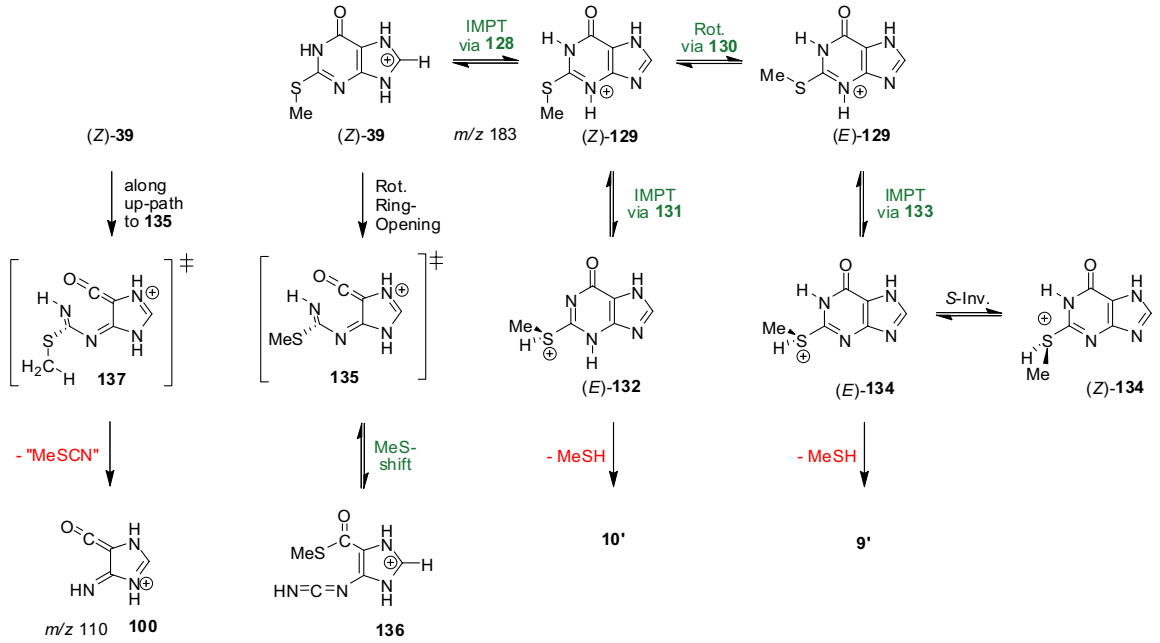

Scheme 9. Major fragmentation paths of protonated thioether **14h**.

ESI-MS of Deoxycytidine

The mass spectrum of electrosprayed deoxycytidine in Figure 1 shows two peaks: the quasi-molecular ion $[\mathbf{3d} + H]^+$ and the fragment $[\mathbf{3h} + H]^+$, *m/z* 112, in which the sugar was replaced by hydrogen. The fragmentation of $[\mathbf{3h} + H]^+$ was studied by MS/MS and the spectrum of Figure 5 is rationalized in Scheme 11õ with reference to the energies of the computed structures shown in Scheme 12.

The proton affinities show that amino group protonation cannot compete with protonation at the carbonyl-O or N3. With **50** present and/or accessible from **51** and **52**, ammonium ion **48** becomes available via transition-state structure **138** with ΔH_{act} = 227.1 kJ/mol. Ion **11h** easily ring-opens to thermodynamically more stable **12h**, protonated (*Z*)-3-isocyanatoacrylonitrile [58].

We also considered options for NH_3 elimination from ring-opened structures and three modes were considered for ring-opening, namely by way of C2–N3 cleavage and rotation of either the amidine unit via **139** or of the protonated isocyanato group via **141** as well as by way of N1–C2 cleavage and rotation of the protonated isocyanato group via **145**. The activation enthalpies ΔH_{act} for the reactions **50** → **139**‡ → **140**, **50** → **141**‡ → **142** → **143**‡ → **144**, and **50** → **145**‡ → **146** are 352.0, 308.2, and 315.9 kJ/mol, respectively, and these energy requirement are too high to compete with the path via **48** (Table 3).

The strong peak with *m/z* 69 shows that protonated cytosine can eliminate isocyanic acid and our potential surface analyses provide information about possible paths for HNCO elimination. The stage is set for HCNO elimination once the N–C bond of **50** is broken along any of the up-paths that lead to the transition-state structures **139**, **141**, and **145**. Actual elimination might occur within wide ranges of the up-paths and well before the respective transition-state region for rotation would be reached. This scenario for HNCO elimination from **50** is related to the eliminations of CN_2H_2 from **23** and of MeSCN from **39**, but it is much less complicated. Only one more CN cleavage has to

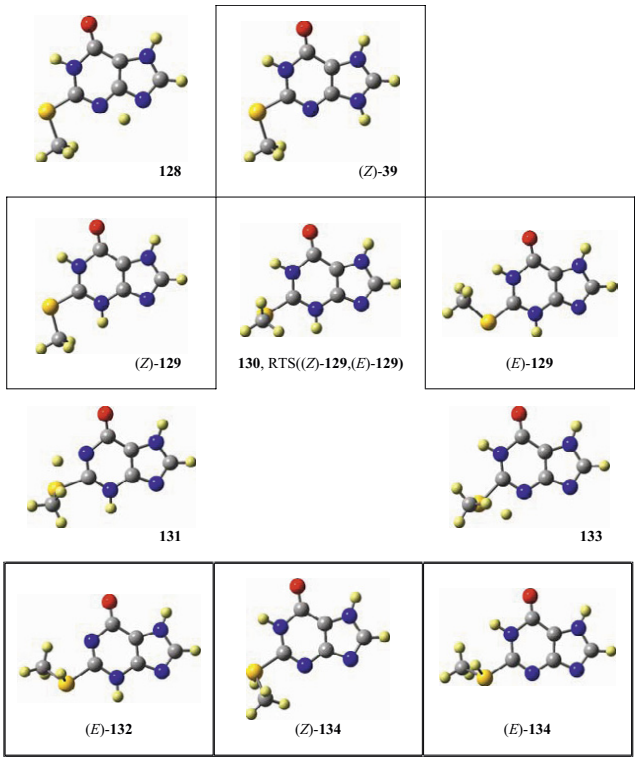

Scheme 10. Paths to sulfonium ions (double-lined) from the conjugate acids of **14h**.

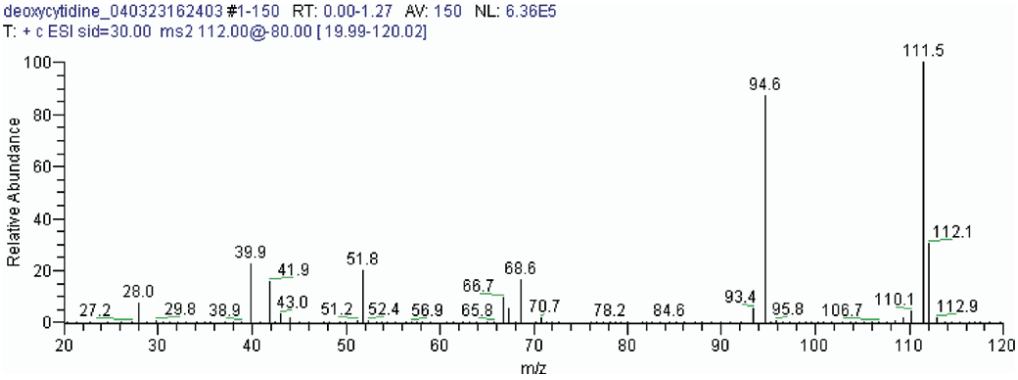

Figure 5. Product-ion spectrum of [**12h** + H]$^+$, *m/z* 112, produced by in-source fragmentation of protonated deoxycytidine.

occur (no additional proton transfer) and 2D-scans (C–N rotational coordinate and C–N bond length) and/or dynamics studies could provide any desired level of mechanistic detail. Considering the energies of the rotational transition-state structures and basic principles of potential energy surface analysis, the up-paths to **141** and **145** appear most suited and these paths also provide consistent rationales for the results of the MS experiments. The elimination of H–N3=C=O along the up-path to **145** would lead to **147** and explain the

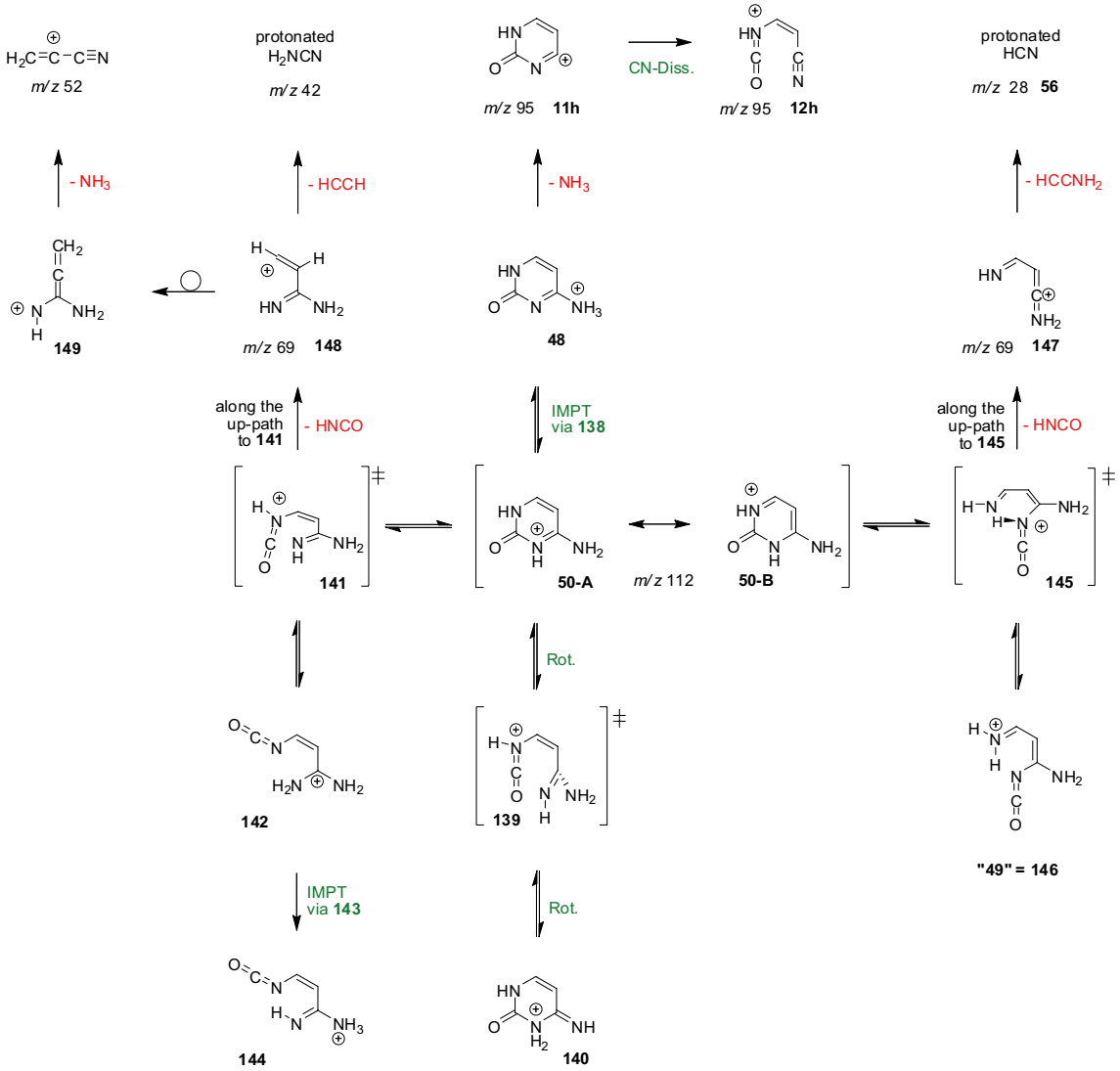

Scheme 11. Major fragmentation paths of protonated cytosine.

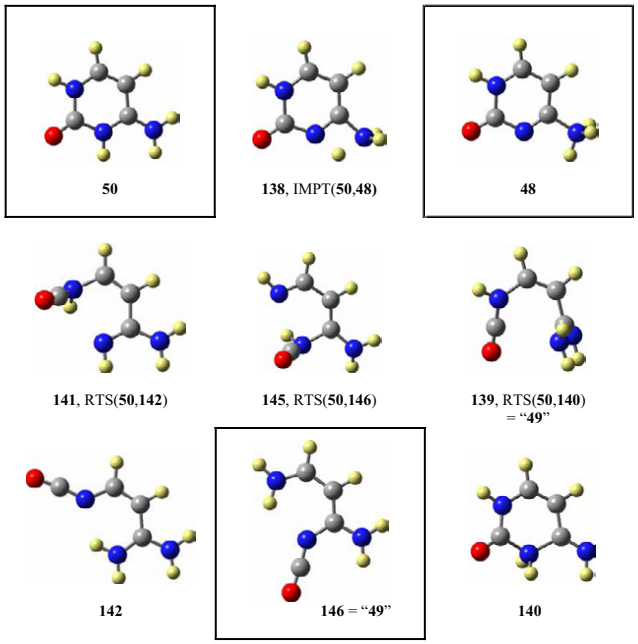

Scheme 12. The N3-protonated cytosine **50** (single-lined) leads to NH_3 elimination from [**3h** + H]$^+$ via ammonium ion **48** (double-lined). Paths involving CN cleavage and rotation via **139, 141,** and **145** also have been explored.

formation of protonated HCN, **56** (*m/z* 28). The elimination of H–N1=C=O along the up-path to **141** would lead to **148** instead and subsequent loss of acetylene would result in protonated cyanamide (*m/z* 42). Alternatively, this mode of HNCO elimination might be followed by 1,2-H-shift to **148** and NH_3 elimination to protonated cyanoacetylene (*m/z* 52).

The study of the fragmentation of 1,3-double ^{15}N-labeled cytidines by Wang et al. [35] revealed the important new finding that NH_3 eliminated from [**3h** + H]$^+$ may contain ^{14}N or ^{15}N. The exchange of the N3- and amino-N atoms was rationalized by the Dimroth rearrangement **50** ⇄ **140** via C2–N3 cleavage and **139**‡ and subsequent proton transfer to reform **50**. To explain the observed excess of unlabeled NH_3 a "small fraction" of the elimination had to be generated by the path **50** → **48** and, hence, that path was thought to compete with the Dimroth rearrangement. While this explanation was perfectly reasonable, the computed activation barriers indicate however a very clear advantage for the path **50** → **48** over the Dimroth rearrangement. Tureček et al. initially considered only N1–C2 cleavage for [**3h** + H]$^+$ and the rearrangement **50** ⇄ **146** via **145**‡ to explain the HNCO elimination [34a]. The labeling results required a reassessment and Tureček et al. [34b] now argued for the rearrangement **50** ⇄ **142** via **141**‡ and NH_3 elimination from **144**. In fact, the authors argued for the

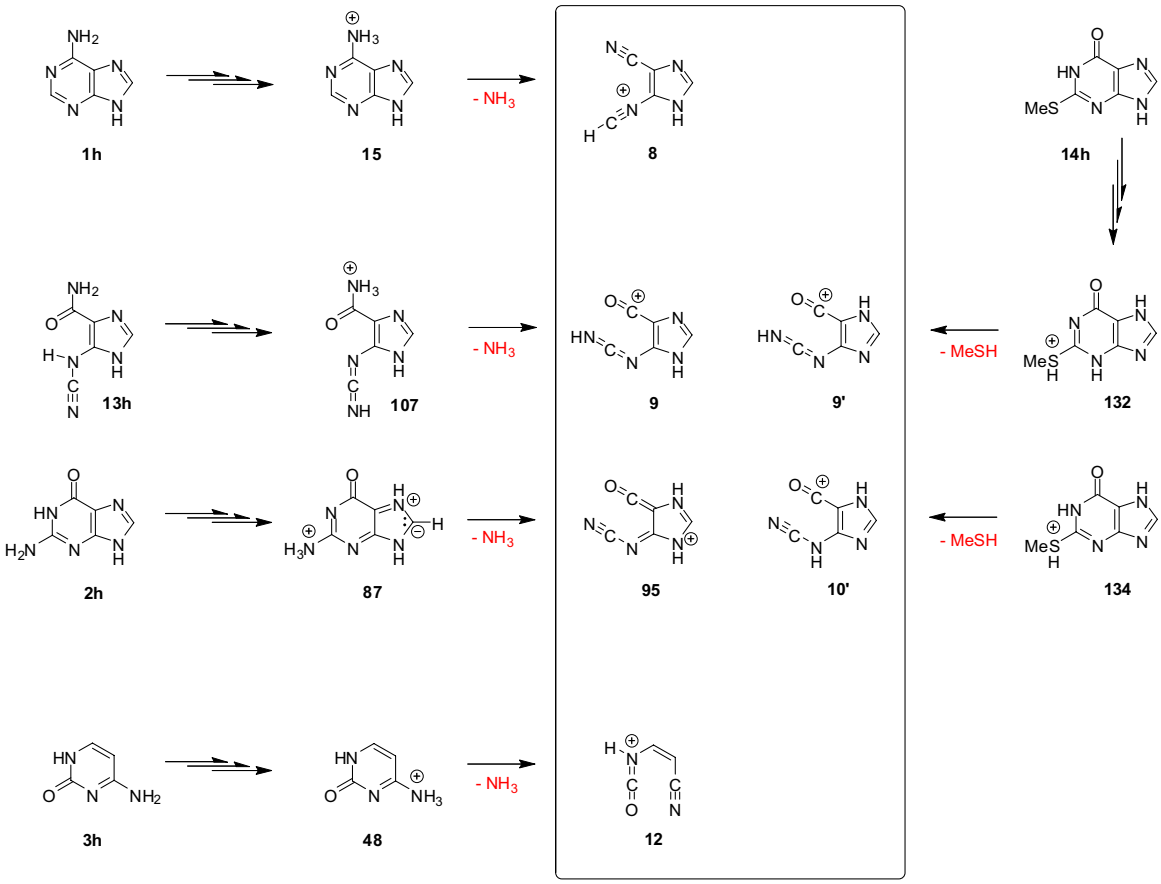

Scheme 13. Summary of results.

exclusive elimination of ammonia from the ring-opened structure **144** and noted that ammonia loss from **48** is endothermic. Yet, one cannot ignore the fact that ΔH_{act}(**50** → **48**) is much smaller than ΔH_{act}(**50** → **141**), that NH_3 elimination from **48** will occur in the mass spectrometer, and that the ammonia elimination is essentially irreversible under those conditions.

To resolve this paradoxical situation requires the accessibility of a mechanism for ammonia elimination that can compete with the reaction **50** → **48** and that accounts for the N-scrambling. We have pointed out that the stage is set for HCNO elimination as soon as one of the N–C bonds of **50** is broken along any of the up-paths leading to the transition state structures **139**‡, **141**‡, and **145**‡ and that the *actual* elimination might occur within wide ranges of the up-paths and well before the respective transition state region for rotation would be reached. This means that the structural possibilities for [**3h** + H]$^+$ are not described in a comprehensive fashion by the conventional consideration of sequences of elemental steps. For example, ion **144** can be formed via intermediate **142** in the sequence outlined in Scheme 11, but this option does not exclude the possibility of formation of **144** directly from **50** via trajectories that do not pass through **142**. To allow for these possible trajectories is not expected to result in any conceptional difference for the outcomes of the reaction of **50** to **146** and/or **147**, for the Dimroth rearrangement of **50**, or for the reaction of **50** to **144**. On the other hand, to consider such trajectories does reveal an interesting alternative for the product palette produced by "the path" from **50** to **149**. There is the obvious possibility that the HNCO and NH_3 eliminations occur in sequence. And one can consider the *additional* scenario in which intramolecular proton transfer and NH_3 elimination occur after N1–C2 cleavage but before HNCO elimination. This region of the potential energy surface of [**3h** + H]$^+$ includes structures resulting by N1–C2 cleavage (without the simultaneous rotations leading toward structures of types **139** or **141**) and it also includes ion-molecule complexes formed by **148** and HNCO. Our analysis suggests, for example, that the acyclic structure **23** discussed in [34b] to explain CO and HNCO eliminations might play a role in NH_3 elimination as well.

Conclusion

MS experiments are rather sensitive to instrument settings (Table 1) and significant quantitative differences in fragmentation modes may occur from one experiment to the next. Nevertheless, our study shows that the protonated nucleobases [**1h** + H]$^+$, [**2h** + H]$^+$, and [**3h** + H]$^+$ can be observed by ESI-MS and that their modes of initial fragmentation can be understood with the knowledge of the tautomer stabilities and the consideration of the paths for intramolecular proton migration. It is for this understanding, that we have confidence in the completeness of our study and we contend that we have observed all of the main modes of initial fragmentation.

We discussed ions **8**–**10** and **12** as possible reactive intermediates in nitrosative deamination chemistry in solution and it has been our aim to provide more direct experimental evidence for the existence of these ions. Hence, we studied NH_3 elimination from the conjugate acids of the nucleobases **1h**–**3h** and models **13h** and **14h**, and the key results are summarized in Scheme 13. Everyone of the postulated ions either was found to exist in the gas phase or to exist in the gas phase as a tautomer. These results provide "semi-direct" experimental evidence for the existence of these ions. The new data go well beyond the "indirect evidence" stemming from inference from mechanistic studies and the additional structural characterization in the MS experiment [59] could provide for "direct" evidence.

The amino group hardly ever is the best protonation site of the substrate, and we discussed possible mechanisms for NH_3 elimination that feature the amino group as the dissociative protonation site. The hydrogen migration is facilitated by electrophilic catalysis, and the standard Lewis structure might obscure the propensity of a hydrogen atom to migration (i.e., **63**, **23**, **50**). Examples have been provided for cases in which the acidic H and the NH_2-group are in a 1,2-relation (**16**, **21**, **22**, **23**, **50**, **63**, **68**, **81**, **105**, **142**), a 1,3-relation (**17**, **28**, **77**, **113**), or a 1,5-relation (**65**, "**30**," "**36**," **33**). This kind of electrophilic catalysis also facilitates the elimination of H_2NCN from **23** and of MeSH and MeSCN from **39**.

Acknowledgments

This study was supported by the United States National Institutes of Health (GM61027). MU Research Support Computing was made possible by Federal Earmark NASA Funds for Bioinformatics Consortium Equipment and additional financial support from Dell, SGI, Sun Microsystems, TimeLogic, and Intel.

References

1. (a) Geiduschek, E. P. Reversible Denaturation of Deoxyribonucleic Acid (DNA). *Proc. Natl. Acad. Sci. U.S.A.* **1961,** *47*, 950–955. (b) Geiduschek, E. P. On the Factors Controlling the Reversibility of DNA Denaturation. J. Mol. Biol. **1962,** *4*, 467–487.
2. Caulfield, J. L.; Wishnok, J. S.; Tannenbaum, S. R. Nitric Oxide-Induced Interstrand Cross-Links in DNA. *Chem. Res. Toxicol.* **2003,** *16*, 571–574.
3. Committee on Nitrite and Alternative Curing Agents in Food. *The Health Effect of Nitrate, Nitrite, and N-Nitroso Compounds*; National Academy Press: Washington, D.C., 1981.
4. Furia, T. E. *Handbook of Food Additives*, 2nd ed.; CRC Press: Cleveland, 1972; pp 150–155.
5. Wakabayashi, K. In *Mutation and the Environment, Part E*; Albertini, R. J.; Ed.; Wiley-Liss, Inc.: New York, 1990; pp 107–116.
6. Culotta, E.; Koshland, D. E. No News is Good News. *Science* **1992,** *258*, 1862–1865.
7. Marnett, L. J. Nitric Oxide: Chemical Events in Toxicity. *Chem. Res. Toxicol*. **1996,** *9*, 807–808.
8. Davis, K. L.; Martin, E.; Turko, I. V.; Murad, F. Novel Effects of Nitric Oxide. *Annu. Rev. Pharmacol. Toxicol*. **2001,** *41*, 203–236.
9. Jackson, A. L.; Loeb, L. A. The Contribution of Endogenous Sources of DNA Damage to the Multiple Mutations in Cancer. *Mutat. Res*. **2001,** *477*, 7–21.
10. Ohshima, H.; Bartsch, H. Chronic Infections and Inflammatory Processes as Cancer Risk Factors: Possible Role of Nitric Oxide in Carcinogenesis. *Mutat. Res*. **1994,** *305*, 253–264.

11. Tamir, S.; Tannenbaum, S. R.The Role of Nitric Oxide (NO) in the Carcinogenic Process.Biochim. Biophys. Acta 1996, 1288, F31–F36.
12. Suzuki, T.; Ide, H.; Yamada, M.; Endo, N.; Kanaori, K.; Tajima, K.; Morii, T.; Makino, K. Formation of 2′-Deoxyoxanosine from 2′-Deoxyguanosine and Nitrous Acid: Mechanism and Intermediates. *Nucleic Acids Res* **2000,** *28*, 544–551.
13. Lucas, L. T.; Gatehouse, D.; Shuker, D. E. G. Efficient Nitroso Group Transfer from N-Nitrosoindoles to Nucleotides and 2′-Deoxyguanosine at Physiological pH. A New Pathway for N-Nitroso Compounds to Exert Genotoxicity. *J. Biol. Chem*. **1999,** *274*, 18319–18326.
14. Dong, M.; Wang, C.; Deen, W. M.; Dedon, P. C. Absence of 2′-Deoxyoxanosine and Presence of Abasic Sites in DNA Exposed to Nitric Oxide at Controlled Physiological Concentrations. *Chem. Res. Toxicol*. **2003,** *16*, 1044–1055.
15. Glaser, R.; Son, M.-S. Pyrimidine Ring Opening in the Unimolecular Dediazoniation of Guanine Diazonium Ion. An ab Initio Theoretical Study of the Mechanism of Nitrosative Guanosine Deamination. *J. Am. Chem. Soc*. **1996,** *118*, 10942–10943.
16. Glaser, R.; Rayat, S.; Lewis, M.; Son, M.-S.; Meyer, S. Theoretical Studies of DNA Base Deamination. 2. Ab Initio Study of DNA Base Diazonium Ions and of Their Linear, Unimolecular Dediazoniation Paths. *J. Am. Chem. Soc*. **1999,** *121*, 6108–6119.
17. Glaser, R.; Lewis, M. Single- and Double-Proton-Transfer in the Aggregate Between Cytosine and Guaninediazonium Ion. *Org. Lett*. **1999,** *1*, 273–276.
18. Glaser, R.; Wu, H.; Lewis, M. Cytosine Catalysis of Nitrosative Guanine Deamination and Interstrand Cross-Link Formation. *J. Am. Chem. Soc*. **2005,** *127*, 7346–7358.
19. Rayat, S.; Glaser, R. 5-Cyanoimino-4-Oxomethylene-dihydroimidazole and Nitrosative Guanine Deamination. A Theoretical Study of Geometries, Electronic Structures, and *N*-Protonation. *J. Org. Chem*. **2003,** *68*, 9882–9892.
20. Rayat, S.; Majumdar, P.; Tipton, P.; Glaser, R. 5-Cyanoimino-4-Oxomethylene-4,5-Dihydroimidazole and 5-Cyanoamino-4-Imidazolecarboxylic Acid Intermediates in Nitrosative Guanosine Deamination. Evidence from (18)O-Labeling Experiments. *J. Am. Chem. Soc*. **2004,** *126*, 9960–9969.
21. Qian, M.; Glaser, R. 5-Cyanoamino-4-Imidazolecarboxamide and Nitrosative Guanine Deamination: Experimental Evidence for Pyrimidine Ring-Opening During Deamination. *J. Am. Chem. Soc*. **2004,** *126*, 2274–2275.
22. Qian, M.; Glaser, R. Demonstration of an Alternative Mechanism for G-to-G Cross-Link Formation. *J. Am. Chem. Soc*. **2005,** *127*, 880–887.
23. Hodgen, B.; Rayat, S.; Glaser, R. Nitrosative Adenine Deamination: Facile Pyrimidine Ring-Opening in the Dediazoniation of Adeninediazonium Ion. *Org. Lett*. **2003,** *5*, 4077–4080.
24. Shuo Yang. *Ammonia Elimination from Protonated Nucleobases. Proton Mobility, Ammonium Ion Formation, and Fragmentation Paths*; M.S. Dissertation, University of Missouri-Columbia, 2007.
25. McLafferty, F. W.; Wachs, T.; Koppel, C.; Dymerski, P. P.; Bockhoff, F. M. *Advances in Mass Spectrometry*, *Vol. VIIb*; Daly, N. R., Ed.; Institute of Petroleum: London, 1978, p. 109.
26. (a) Koch, W.; Holthausen, M. C. *A Chemist's Guide to Density Functional Theory*, *2nd ed.*; Wiley-VCH: Weinheim, 2001. (b) Parr, R. G; Weitao, Y. *Density-Functional Theory of Atoms and Molecules*; International Series of Monographs on Chemistry. Oxford University Press: Oxford, UK, 1994.
27. Frisch, M. J.; Trucks, G. W.; Schlegel, H. B.; Scuseria, G. E.; Robb, M. A.; Cheeseman, J. R.; Montgomery, J. A., Jr.; Vreven, T.; Kudin, K. N.; Burant, J. C.; Millam, J. M.; Iyengar, S. S.; Tomasi, J.; Barone, V.; Mennucci, B.; Cossi, M.; Scalmani, G.; Rega, N.; Petersson, G. A.; Nakatsuji, H.; Hada, M.; Ehara, M.; Toyota, K.; Fukuda, R.; Hasegawa, J.; Ishida, M.; Nakajima, T.; Honda, Y.; Kitao, O.; Nakai, H.; Klene, M.; Li, X.; Knox, J. E.; Hratchian, H. P.; Cross, J. B.; Bakken, V.; Adamo, C.; Jaramillo, J.; Gomperts, R.; Stratmann, R. E.; Yazyev, O.; Austin, A. J.; Cammi, R.; Pomelli, C.; Ochterski, J. W.; Ayala, P. Y.; Morokuma, K.; Voth, G. A.; Salvador, P.; Dannenberg, J. J.; Zakrzewski, V. G.; Dapprich, S.; Daniels, A. D.; Strain, M. C.; Farkas, O.; Malick, D. K.; Rabuck, A. D.; Raghavachari, K.; Foresman, J. B.; Ortiz, J. V.; Cui, Q.; Baboul, A. G.; Clifford, S.; Cioslowski, J.; Stefanov, B. B.; Liu, G.; Liashenko, A.; Piskorz, P.; Komaromi, I.; Martin, R. L.; Fox, D. J.; Keith, T.; Al-Laham, M. A.; Peng, C. Y.; Nanayakkara, A.; Challacombe, M.; Gill, P. M. W.; Johnson, B.; Chen, W.; Wong, M. W.; Gonzalez, C.; and Pople, J. A. *Gaussian 03, Revision D. 01*; Gaussian, Inc.: Wallingford CT, 2004.
28. Rice, J. M.; Dudek, G. O. Mass Spectra of Nucleic Acid Derivatives. II. Guanine, Adenine, and Related Compounds. *J. Am. Chem. Soc*. **1967,** *89*, 2719–2725.
29. Barrio, M. C. G.; Scopes, D. I. C.; Holtwick, J. B.; Leonard, N. J. Syntheses of all Singly Labeled [15N]-Adenines: Mass Spectral Fragmentation of Adenine. *Proc. Natl. Acad. Sci. U.S.A*. **1981,** *78*, 3986–3988.
30. Sethi, S. K.; Gupta, S. P.; Jenkins, E. E.; Whitehead, C. W.; Townsend, L. B.; McCloskey, J. A. Mass Spectrometry of Nucleic Acid Constituents. Electron Ionization Spectra of Selectively Labeled Adenines. *J. Am. Chem. Soc*. **1982,** *104*, 3349–3353.
31. Rice, J. M.; Dudek, G. O.; Barber, M. Mass Spectra of Nucleic Acid Derivatives Pyrimidines. *J. Am. Chem. Soc*. **1965,** *87*, 4569–4576.
32. Fryèák, P.; HušKová, R.; Tomáš, A.; Lemr, K. Atmospheric Pressure Ionization Mass Spectrometry of Purine and Pyrimidine Markers of Inherited Metabolic Disorders. *J. Mass Spectrom*. **2002,** *37*, 1242–1248.
33a. Wilson, M. S.; McCloskey, J. A. Chemical ionization mass spectrometry of nucleosides. Mechanisms of ion formation and estimations of proton affinity. *J. Am. Chem. Soc*. **1975,** *97*, 3436–3444.
33b. Nelson, C. C.; McCloskey, J. A. Collision-Induced Dissociation of Adenine. *J. Am. Chem. Soc*. **1992,** *114*, 3661–3668.
33c. Gregson, J. M.; McCloskey, J. A. Collision-Induced Dissociation of Protonated Guanine. *Int. J. Mass Spectrom. Ion Processes* **1997,** *165/166*, 475–485.
34a. Yao, C.; Cuadrado-Peinado, M. L.; Polasek, M.; Tureček, F. Gas-phase tautomers of protonated 1-methylcytosine. Preparation, energetics, and dissociation mechanisms. *J. Mass Spectrom*. **2005,** *40*, 1417–1428.
34b. Yao, C.; Tureček, F.; Polce, M. J.; Wesdemiotis, C. Proton and hydrogen atom adducts to cytosine. An experimental and computational study. *Int. J. Mass Spectrom*. **2007,** *265*, 106–123.
35. Cao, H.; Wang, Y. Collisionally Activated Dissociation of Protonated 2′-Deoxycytidine, 2′-Deoxyuridine, and their Oxidatively Damaged Derivatives. *J. Am. Soc. Mass. Spectrom*. **2006,** *17*, 1335–1341.
36. Tureček, F.; Chen, X. Protonated Adenine: Tautomers, Solvated Clusters, and Dissociation Mechanisms. *J. Am. Soc. Mass Spectrom*. **2005,** *16*, 1713–1726.
37. Curtiss, L. A.; Redfern, P. C.; Frurip, D. J. Theoretical Methods for Computing Enthalpies of Formation of Gaseous Compounds. *Rev. Comput. Chem*. **2000,** *15*, 147–211.
38. Giese, B.; McNaughton, D. Density Functional Theoretical (DFT) and Surface-Enhanced Raman Spectroscopic Study of Guanine and Its Alkylated Derivatives. Part 1. DFT Calculations on Neutral, Protonated, and Deprotonated Guanine. *Phys. Chem. Chem. Phys*. **2002,** *4*, 5161–5170.
39. Jang, Y. H.; Goddard, W. A., III; Noyes, K. T.; Sowers, L. C.; Hwang, S.; Chung, D. S. pK_a Values of Guanine in Water: Density Functional Theory Calculations Combined with Poisson-Boltzmann Continuum-Solvation Model. *J. Phys. Chem. B* **2003,** *107*, 344–357.
40. Greco, F.; Liguori, A.; Sindona, G.; Uccella, N. Gas-Phase Proton Affinity of Deoxyribonucleosides and Related Nucleobases by Fast Atom Bombardment Tandem Mass Spectrometry. *J. Am. Chem. Soc*. **1990,** *112*, 9092–9096.
41. Chandra, A. K.; Nguyen, M. T.; Uchimaru, T.; Zeegers-Huyskens, T. Protonation and Deprotonation Enthalpies of Guanine and Adenine and Implications for the Structure and Energy of Their Complexes with Water: Comparison with Uracil, Thymine, and Cytosine. *J. Phys. Chem. A* **1999,** *103*, 8853–8860.
42. Taft, R. W. *Proton Transfer Reaction*; Caldin, E. F., Gold, V., Eds.; Wiley-Halstead: New York, 1975; Chap II.
43. Lias, S. G.; Bartmess, J. E.; Liebman, J. F.; Holmes, J. L.; Levin, R. D.; Mallard, W. G. Gas-Phase Ion and Neutral Thermochemistry. *J. Phys. Chem. Ref. Data* **1988**, (*Suppl. 1*), 17.
44. Karpas, Z.; Berant, Z.; Stimac, R. M. An Ion Mobility Spectrometry/Mass Spectrometry (IMS/MS) Study of the Site of Protonation in Anilines. *Struct. Chem*. **1990,** *1*, 201–204.
45. Flammang, R.; Dechamps, N.; Pascal, L.; Van Haverbeke, Y.; Gerbaux, P.; Nam, P.-C.; Nguyen, M. T. Ring Versus Nitrogen Protonation of Anilines. *Lett. Org. Chem*. **2004,** *1*, 23–30.
46. Tu, Y.-P. Dissociative Protonation Sites: Reactive Centers in Protonated Molecules Leading to Fragmentation in Mass Spectrometry. *J. Org. Chem*. **2006,** *71*, 5482–5488.
47. Paizs, B.; Suhai, S. Fragmentation Pathways of Protonated Peptides. *Mass Spectrom. Rev*. **2005,** *24*, 508–548.
48. Mouls, L.; Subra, G.; Aubagnac, J.-L.; Martinez, J.; Enjalbal, C. Tandem Mass Spectrometry of Amidated Peptides. *J. Mass Spectrom*. **2006,** *41*, 1470–1483.
49. Csonka, I. P.; Paizs, B.; Suhai, S. Modeling of the Gas-Phase Ion Chemistry of Protonated Arginine. *J. Mass Spectrom*. **2004,** *39*, 1025–1035.
50. Cooper, T.; Talaty, E.; Grove, J.; Van Stipdonk, M.; Suhai, S.; Paizs, B. Isotope Labeling and Theoretical Study of the Formation of a3* Ions from Protonated Tetraglycine. *J. Am. Soc. Mass Spectrom*. **2006,** *17*, 1654–1664.
51. Glaser, R.; Hodgen, B.; Farrelly, D.; McKee, E. Adenine Synthesis in Interstellar Space: Mechanisms of Prebiotic Pyrimidine Ring-Formation in Monocyclic HCN-Pentamers. *Astrobiology* **2007,** *7*, 455–470.
52. Morgan, K. M. Reaction mechanisms. Part III. Pericyclic reactions. *Annu. Rep. Prog. Chem. B* **2005,** *101*, 284–304.
53. Tordini, F.; Bencini, A.; Bruschi, M.; Gioai, L. D.; Zampella, G.; Fantucci, P. Theoretical Study of Hydration of Cyanamide and Carbodiimide. *J. Phys. Chem. A* **2003,** *107*, 1188–1196.
54. Polce, M. J.; Kim, Y.; Wesdemiotis, C. First Experimental Characterization of Aminocarbene. *Int. J. Mass Spectrom. Ion Processes* **1997,** *167/168*, 309–315.
55. Lin, H. Y.; Ridge, D. P.; Uggerud, E.; Vulpius, T. Unimolecular Chemistry of Protonated Formamide. Mass Spectrometry and ab Initio Quantum Chemical Calculations. *J. Am. Chem. Soc*. **1994,** *116*, 2996–3004.
56. Marynick, D. S.; Scanion, K.; Eades, R. A.; Dixon, D. A. Absolute Proton Affinities of PH_3 and H_2S. *J. Phys. Chem*. **1981,** *85*, 3364–3366.
57. Haney, M. A.; Franklin, J. L. Mass Spectrometric Determination of the Proton Affinities of Various Molecules. *J. Phys. Chem*. **1969,** *73*, 4328–4331.
58. Glaser, R.; Wu, H.; von Saint Paul, F. Chemical Carcinogens in Nonenzymatic Cytosine Deamination: 3-Isocyanatoacrylonitrile. *J. Mol. Model*. **2006,** *12*, 731–737.
59. Cooper, H. J.; Hakansson, K.; Marshall, A. G. The Role of Electron Capture Dissociation in Biomolecular Analysis. *Mass Spectrom. Rev*. **2005,** *24*, 201–222.